Chapter 5 High-frequency vibration and ultrasonic processing

D.G. Eskin, I. Tzanakis

5.1 Historical overview of ultrasonic cavitation science and applications

The application of ultrasound to the processing of liquids and slurries has a long history. The theory of oscillations was developed by Lord Rayleigh who laid the foundation for nonlinear acoustics. He also theoretically quantified the pressure pulse resulted from the imploding cavitation bubble and suggested that the acoustic pressure is directly related to the wave energy and velocity [1], which was experimentally confirmed by W.J. Altberg [2]. Significant contribution to the theory of cavitation was made by Ya.I. Frenkel [3] and E.N. Harvey [4] who explained why the cavitation threshold in liquids is well below the theoretical tensile strength of the liquid phase, suggesting a model of cavitation nuclei in real liquids as stable gas pockets at the surface imperfections of suspended particles. The pulsation of a cavitation bubble was described analytically by B.E. Nolting and E.A. Neppiras [5]. They introduced the resonance radius of the bubble. The bubble smaller that and around the resonance size will rapidly grow and then implode within one or two sound wave cycles. Each of the imploded bubble will generate large pressure pulse and create many even smaller bubbles, starting a chain reaction of bubble multiplication. The bubble larger than the resonance size will not implode but, being relatively stable, will pulsate around its size. The product of the number of cavitation bubbles in the unit volume and the maximum volume of a single bubble is called cavitation index. When this index approaches unity the amount of bubbles in the unit volume becomes so big that they substitute the liquid phase and the ultrasonic power transmitted to the liquid declines rapidly [6, 7]. This is the base of so-called shielding effect of the cavitation region, when the acoustic energy rapidly attenuates within the cavitation zone and does not propagate to the liquid volume.

The practical aspects of ultrasonic cavitation started to attract the attention of physicists, chemists and other applied scientists and researchers. R. Wood and A. Loomis (1927) observed intensive acoustic streaming and fountaining, ultrasonic degassing, emulsification and atomization, cavitation damage of organic tissue, etc. [8].

The direct observation of cavitation became possible with the development of high-speed film cameras, high-brilliance impulse lamps and, eventually, laser illumination in the 1950s–1960s [9, 10, 11, 12, 13, 14]. The images taken with the exposure 0.5 to 5 msec enabled the

in-situ study of the cavitation development, bubbles collapse and sonoluminescence. In recent years, in-situ studies of cavitation in liquid metals became possible using synchrotron radiation [15, 16, 17].

The application of vibrations to treating metals dates back to the 1870s when D.K. Chernov reported that shaking molten steel solidifying in a mold resulted in the formation of very fine crystals [18]. The effects of low-frequency vibration on liquid and solidifying metals were reviewed by G.F. Balandin [19] and J. Campbell [20].

The ultrasonic processing of liquid and solidifying metals has been reviewed on numerous occasions, e.g. by E.A. Hiedemann (1954) [21], G.I. Eskin (1961, 1965) [22, 23], H.G. Flinn (1964) [24], H.J. von Seemann et al. (1967) [25], O.V. Abramov and I.I. Teumin (1970) [26], O.A. Kapustina (1970) [27], O.V. Abramov (1972) [28], K. Buxmann (1972) [29], and J. Campbell (1981) [20].

Extensive studies on solidification of various metals and alloys under ultrasonic fields of different frequencies and intensities were performed by Seemann et al. [25, 30, 31,] and G. Schmid et al. [32, 33] in the 1930s–1940s. A significant refining of grain structure was achieved in these experiments, and crystal fragmentation was suggested to be responsible [33]. At the same time a group of scientists advocated the cavitation-induced nucleation of the solid phase [34, 35, 36, 37]. V.I. Danilov and B.M. Teverovsky [36] suggested cavitation-assisted heterogeneous nucleation through activation of insoluble impurities. A.P. Kapustin observed the formation of new crystallization centers under sonication of very pure liquids, hence – something different from activation of impurities might have happened [26]. J.D. Hunt and K.A. Jackson [38] demonstrated through calculations and dedicated experiments on water that the collapse of cavitation bubbles and the resultant surge of pressure might be responsible for the nucleation due the local change of phase equilibria, increase of the melting point (by tens of degrees!), and the effective local undercooling.

The application of ultrasound to processing of commercial alloys started with the works of Seemann et al. (e.g. [31]) who demonstrated efficient refinement of the duralumin ingot grain structure and an improvement of its mechanical properties. This group also reported structure refinement of tin and zinc [25] as well as brass and steel [25, 39]. G.I. Eskin [23] applied ultrasonic cavitation treatment to a variety of model and commercial foundry Al alloys (hypo- and hypereutectic Al–Si alloys), and demonstrated that the grain structure, Gintermetallics and primary crystals were refined under cavitation conditions. Later

ultrasonic processing was shown to be advantageous for receiving refined grain structure and improved mechanical properties of direct-chill (DC) cast wrought magnesium alloys [40].

The proper choice of the material for sonotrodes (horns, ultrasonic tips) was treated with special care, and Nb and its alloys were recommended for use in molten aluminum [23]. Direct introduction of ultrasound to high-temperature melts is, however, almost impossible. Consumable steel horns were reported to be used to treat Fe-based alloys [28]. Indirect ways were tested including transmission of the oscillations via mold, through solid substrate upon ark vacuum remelting, or through the layer of molten slag upon electro-slag remelting [41, 42]. Most recently a contactless excitation of cavitation in liquid aluminum through a combination of induction coils was developed [43]. Such indirect ways open the way to treat virtually all metals.

An important effect of ultrasonic vibrations and cavitation that attracted the interest of metallurgists was degassing of the melt. The nature of ultrasonic degassing was first revealed on water. O. Lindström [44] suggested that the ultrasonic degassing of water is due to the diffusion of dissolved oxygen into the cavitation bubbles, their oscillation and growth and, finally flotation to the surface. Kapustina [27] concluded that the most important role is played by the oscillations of the bubbles in the acoustic field, while ultrasonic cavitation takes the supportive role in intensification of the bubble formation and acceleration of bubble/liquid interfacial diffusion. G.I. Eskin [23] argued that the cavitation is essential for ultrasonic degassing of metallic melts where the natural gas bubbles are not typically present, unlike those in water. Therefore, the formation and multiplication of bubbles (essential for degassing) can be only achieved by cavitation.

Another important effect of ultrasound is atomization and dispersion of liquid and solid phases with obvious metallurgical applications in manufacturing composite materials as well as immiscible alloys. Schmid and Ehret [32] and Becker [45] described Al–Pb and Zn–Pb alloys produced with ultrasonic melt processing as stable suspensions. Nonmetallic and solid particles can also be introduced into liquid metals, forming metal-matrix composites. G.I. Pogodin-Alekseev and V.V. Zaboleev-Zotov reported in 1958 the introduction of particulate (from 2–20 μm) alumina, silicon carbide, and titanium nitride in liquid aluminum in quantities of 10 to 50 wt% [46]. Seemann and Staats published in 1968 an important paper where they summarized their earlier works on the dispersion of metallic (Ti, Fe) and ceramic (carbides, oxides) particles in molten aluminum using 20-kHz magnetostrictive transducer and an alumina sonotrode [47].

E. Herrmann described, already in 1958, many pilot installations for ultrasonic treatment of molten metal [48]. The versatility of the treatment was illustrated by examples with ultrasonic processing conducted in the furnace, melt flow, feeders of castings, and in the molds with the aim to remove dissolved gases, refine structure, and improve casting properties.

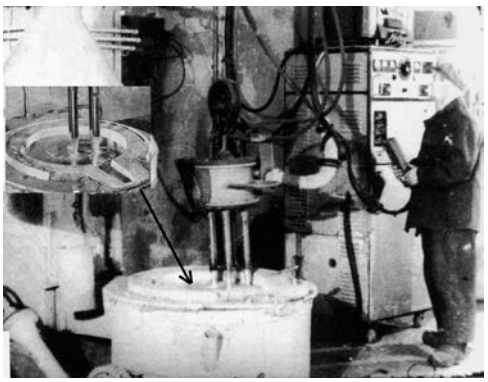

Figure 5.1. Aluminum degassing by submerged sonotrodes in the 1960s (courtesy of G.I. Eskin).

One of the early pilot-scale trials of ultrasonic melt processing of aluminum alloys during aluminum semi-continuous casting was described by Seemann and Menzel in 1947 [31]. Commercial size (290 mm) billets from a duralumin (AA2024) were cast with ultrasonic processing of the melt in the sump of the billet. In these experiments a powerful ultrasonic generator (up to 25 kW) exciting four 2-kW magnetostrictive transducers at 40 kHz. The efficiency of the entire assembly was 14 percent and it was able to deliver an intensity of 2.0 W/cm^2 to the cross-sectional area of the billet (660 cm^2), which was sufficient to achieve grain refinement, reduced porosity, and increased ultimate strength.

The first industrial ultrasonic degassing installation (UZD-200) was developed in 1959 to treat 100–200 kg of melt in a crucible before casting [23]. The UZD-200 unit included a l0-kW lamp ultrasonic generator and a special switching circuit allowed for the alternate operation of four magnetostrictive transducers with Ti or Nb sonotrodes, Fig. 5.1. Similar installations were used for DC casting of aluminum alloys when the ultrasonic treatment was performed in the sump of a billet or in the launder [50].

This brief historical overview shows that the ultrasonic melt processing has a long tradition. It originated from advances in physics that led to the design of modern equipment; followed

by technological developments and trials that started in the 1930s and continued through the 1980s, leading to the first industrial implementations.

5.2 Brief theoretical introduction to ultrasonic cavitation processing

Generally acoustic phenomena are classified with respect to their frequencies: ultrasound is commonly bordered on the lower side by 16000 Hz. Commercial ultrasonic transducers are capable of generating power densities about 10^5–10^6 W/m^2 at frequencies of 18–20 kHz, which is sufficient for treatment of liquid and solidifying melts. High-frequency transducers (up to the MHz range) are also commercially available and are typically used in cleaning and chemical processing.

When a source of ultrasonic oscillations is introduced into the liquid pool it induces an ultrasonic field whose characteristics depend on the oscillation parameters and on the properties of the treated medium.

One of the basic parameters is the propagation velocity of elastic oscillations. This velocity is governed by the physical properties of the medium where the wave propagates. At a given temperature, the velocity [m/s] of (ultra)sonic longitudinal waves in the solid phase with density ρ, Young's modulus E, and Poisson's ratio μ_P is determined by

$$c = \sqrt{\frac{E(1-\mu_P)}{[\rho(1+\mu_P)(1-2\mu_P)]}}. \qquad (5.1)$$

In the liquid phase, where elastic properties depend on the compressibility, the velocity of acoustic wave can be determined from

$$c = \sqrt{1/(\beta_{ad}\rho)}, \qquad (5.2)$$

where ρ is the liquid density and β_{ad} is the adiabatic compressibility. For gases, the molecular motion is related to the adiabatic index $\gamma = c_p/c_v$ (the ratio of specific heats at constant pressure and volume), gas pressure P_0, and density ρ:

$$c = \sqrt{\gamma P_0/\rho}. \qquad (5.3)$$

Generated at any point in the medium (solid, fluid, or gas), oscillating disturbances propagate through the medium as elastic waves of alternating compressions and rarefactions. As follows from Eqs. (5.1)–(5.3), the velocity of elastic waves in an unbound medium is independent of the frequency and, up to certain magnitudes, of the intensity (this relation is referred to as the linear approximation).

The product of propagation velocity c and density ρ (ρc) is called the wave (or acoustic) impedance of the given medium. It is equal to

$$\rho c = P_A/v = P/2\pi f A, \qquad (5.4)$$

where P_A is the sound pressure in the travelling wave and v is its oscillation velocity that is determined by frequency f and amplitude A of the oscillations. Here $2\pi f$ is called angular velocity ω.

The sound pressure P_A, therefore, can be expressed as

$$P_A = v\rho c = \rho c A_0 \omega \cos(\omega t - \frac{\omega x}{c}) \qquad (5.5)$$

A very important parameter of the ultrasonic field determining to a great extent the efficiency of processing is the ultrasonic intensity I, or power flux W_a normalized by area S. In the simplest case of a plane wave, the intensity [W/m^2] is given by

$$I = \frac{W_a}{S} = \frac{1}{2}\rho c v^2 = \frac{1}{2}\rho c (A_0\omega)^2 = \frac{1}{2} P_A v \qquad (5.6)$$

The acoustic intensity is, therefore, proportional to the squared amplitude and frequency, which to a great extent determines the selection of processing equipment and regimes.

When cavitation develops in the melt, the temporal characteristics of force and velocity at the sonotrode radiating face and in the melt containing cavitation bubbles vary, so Eqs. (5.5) and (5.6) may be used to describe the actual technological processes of melt sonication only in the first, or linear, approximation.

In the presence of cavitation, the acoustic impedance of the melt that is a function of oscillation amplitude or velocity rapidly decreases, as the sound velocity and the pressure in the cavitating liquid phase is no longer the same as in the non-cavitating liquid. The intensity or transmitted power can still be considered proportional to the squared oscillation velocity, but with the acoustic impedance rapidly decreasing after the cavitation threshold has been reached.

Figure 5.2 shows the dimensionless parameter K, which is the ratio of acoustic impedance under cavitation to the acoustic impedance in the absence of cavitation, versus the oscillating amplitude of the sonotrode at 18 kHz for water (*1*) [49] and aluminum melt (2) [50]. When the null-to-peak amplitude exceeds 0.5 μm for water at 20°C and 2–3 μm for an aluminum melt, the wave resistance decreases to values ten times smaller than for sonication without cavitation.

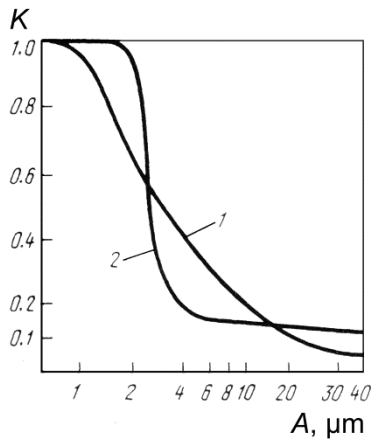

Figure 5.2. Relative acoustic impedance ***K*** versus the amplitude ***A*** of the sonotrode at 18 kHz. (1) water; and (2) aluminum melt (after [50]).

On the other hand, when acoustic cavitation begins, the acoustic power transferred to the fluid increases. Figure 5.3 gives the relation between the oscillation amplitude and the acoustic power generated by standard ultrasonic equipment and transmitted into an aluminum melt of commercial purity at a resonance frequency of 18 kHz for different surface areas of the sonotrode radiating face.

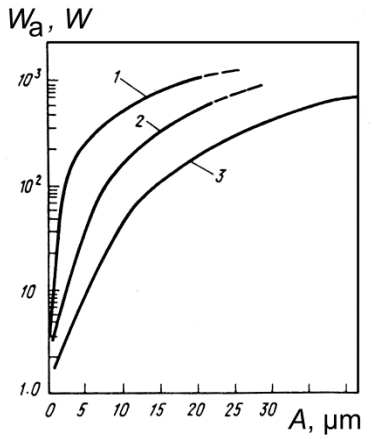

Figure 5.3. Power W_a transferred into the melt versus the amplitude A of the sonotrode at a resonance frequency of 18 kHz for three sonotrode diameters: (1) 65 mm, (2) 40 mm, and (3) 20 mm (after [50]).

Only recently the instrumental facilities have been developed that allow the measurements of cavitation activity in liquid aluminum [51, 52, 53], whereas the evaluation

of flow patterns and detailed study of cavitation are still mostly reserved to transparent liquids and, increasingly, to computer modeling and simulation.

The propagation of ultrasound is accompanied with losses of oscillation energy. The amplitude and intensity of a plane ultrasonic wave decrease exponentially with the propagation distance ***x:***

$$A = A_0 e^{-ax}, \qquad (5.7)$$

$$I = I_0 e^{-2ax}, \qquad (5.8)$$

where α is the loss coefficient or sound absorption, or attenuation factor.

Recent studies in Al melt [54] showed that the variation of the maximum pressure with distance from the sonotrode surface obeys a power law (Figure 5.4). The decay of pressure with distance is with an exponent of 1.45 per meter. This pressure dependence on distance is in agreement with quantitative experimental observations with a high-temperature cavitometer [52] also plotted in Fig. 5.4, with a decay exponent of 1.28 per meter [55]. The experimental values are quoted in mV (pressures can be different as shown in Fig. 5.5 due to the shielding effect [56]). This large decay is expected, as the efficiency in acoustic radiation is proportional to the ratio of horn radius to wavelength. The large wavelength in aluminum and the comparatively small sonotrode makes the pressure decrease with distance more pronounced.

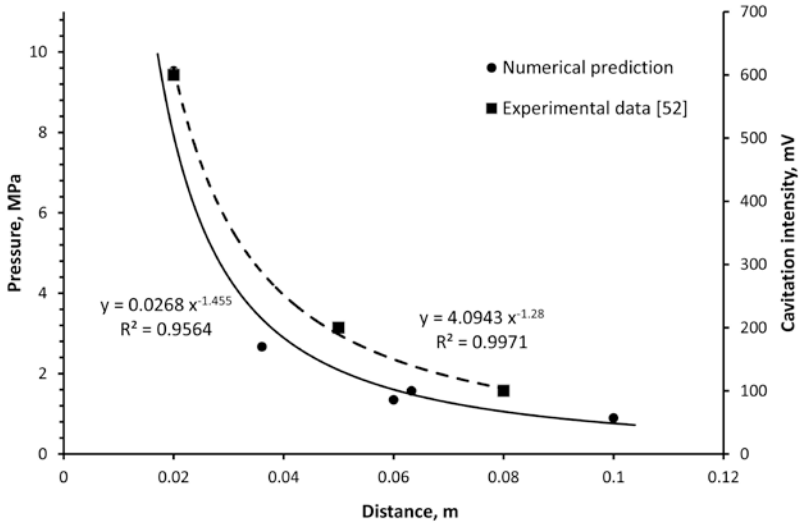

Figure 5.4. Attenuation of acoustic pressure (calculated numerically in MPa and experimentally measured as intensity) in liquid aluminum with the distance from the sonotrode (ultrasonic frequency 17.7 kHz).

Apart from distance, which according to [55] plays a predominant role (74% of contribution) in attenuating cavitation intensity and hence the efficiency of cavitation treatment in the melt alloy, acoustic power and melt temperature also affect the cavitation development in the melt with the corresponding contributions of 14 and 12%.

The absorption of ultrasound in the liquid phase is related to the viscosity and thermal conductivity of the melt, and changes with the ultrasound frequency. The attenuation factor depends on the squared frequency:

$$\alpha = \frac{\omega^2}{2\rho c^3}\left(\frac{4}{3}\mu + \mu' + a\left(\frac{1}{c_v} - \frac{1}{c_p}\right)\right), \qquad (5.9)$$

where μ and μ' are the shear and volume viscosities; a is the thermal conductivity, and c_v and c_p are the specific heats at constant volume and pressure, respectively. This dependence demonstrates that very high ultrasonic frequencies would be impractical for melt processing because of their strong attenuation (even without taking into account the shielding effect of the developed cavitation region).

In addition to that, non-dimensional analysis of an ultrasonically treated aluminum melt showed that heat conductivity would be the dominant heat transfer process over convection, and the attenuation of the acoustic waves propagation (sound converts to heat) in this medium is significant [57]. On the other hand, same report showed that in non-metallic liquids that are good heat insulators the heat dissipation will be controlled by viscous forces (convection).

The interfaces between the liquid phase and suspended particles (non-metallic inclusions, and crystals) may significantly affect absorption [58]. The attenuation factor increases with the amount of particles and with their fineness. Similar effect is produced by gas bubbles whose interfaces with the melt act as scattering sources. As we will show below, the very same interfaces of gaseous and solid inclusions act as cavitation nuclei and favor the development of cavitation which absorbs additional ultrasonic energy.

Cavitation development in water closely resembles to that of liquid aluminium [57]. This allows researchers to experimentally investigate cavitation activity in water using advanced experimental equipment and techniques such as advanced cavitometers and particle image velocimetry (PIV) and subsequently feed numerical models to replicate and validate the cavitation development in liquid aluminum [54].

Tzanakis et al. [53] directly measured cavitation acoustic pressures in liquid aluminum using an advanced high temperature cavitometer (Fig. 5.5). Results showed that shielding and acoustic damping is more pronounced in liquid aluminum, in contrast to a more consistent

pressure regime measured in water. The extent of the cavitation zone was quantified in both tested liquids.

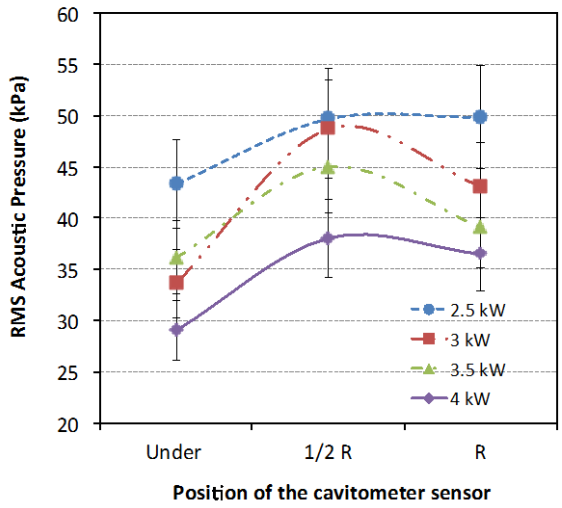

a

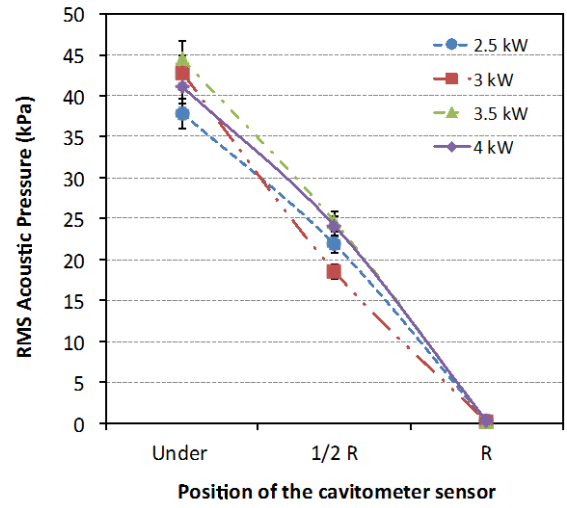

b

Figure 5.5. Variation in RMS acoustic pressures of the driving frequency (17 kHz) at three different positions (under the sonotrode, at 1/2*R* and at *R* from the source) across the crucible in (a) water and (b) liquid Al. (I. Tzanakis, D. Eskin, 2015).

According to well-adopted views on the cavitation threshold, the tensile stress-induced disruptions in liquids are not governed by molecular forces, but rather by the presence of cavitation nuclei such as vapor and gas bubbles, solid gas-adsorbing suspensions, and hydrophobic inclusions.

The cavitation strength is related to the surface tension at the liquid-gas interface and the initial bubble radius. The viscosity μ also markedly influences the cavitation response of the liquid, increasing the cavitation threshold and the critical resonance radius of a cavitation bubble. The cavitation threshold or critical pressure is directly proportional to the ln(μ) [59] or to μ [60].

The dynamic behavior of a single vapor-gas cavity in an uncompressible liquid is described (neglecting gas diffusion to the cavity) by the Noltlingk–Neppiras equation [61]:

$$\rho\left(\ddot{R}R+\frac{3}{2}\dot{R}^2\right)+\ 4\mu\frac{\dot{R}}{R}+\frac{2\sigma}{R}-\left(P_0-P_v+\frac{2\sigma}{R_0}\right)\left(\frac{R_0}{R}\right)^3+\ P_0-P_v-P_A\sin(\omega t)=0 \quad (5.10)$$

Here, R is the radius of the cavity, R_0 is the initial radius of the cavity, σ is the surface tension of the melt, μ is the viscosity of the melt, ρ is the melt density, P_v is the vapor

pressure, P_A is the sound pressure, P_0 is the static ambient pressure, and $\omega = 2\pi f$ is the angular velocity.

The critical radius of a cavitation bubble can be related to the surface tension σ and viscosity μ of the liquid phase as

$$R_{cr} = \left(\frac{3\kappa-1}{3\kappa}\right)\frac{\sigma}{P_g}\left[-1+\sqrt{1+\frac{24\kappa\mu^2 P_g}{(3\kappa-1)^2\sigma^2\rho}}\right], \qquad (5.11)$$

where κ is the polytropic exponent varying from 1 to c_p/c_v [62], P_g is the initial gas pressure and ρ is the liquid density [63].

Neglecting the surface tension, the critical radius depends directly on the liquid viscosity [63]:

$$R_{cr} = \frac{2\sqrt{2\mu}}{\sqrt{3\kappa P_g \rho}}. \qquad (5.12)$$

This critical radius can also be described as [64]:

$$R_{cr} = \sqrt{\frac{9kT_b \mathbf{R} m_g}{8\pi\sigma}}, \qquad (5.13)$$

where k is the Boltzman constant, **R** is the gas constant, m_g is the mass of gas inside the bubble, and T_b is the temperature of the bubble. The bubbles smaller than the critic radius will be stable.

The resonance radius R_r has been defined from the Minnaert resonance condition [65]:

$$f = \frac{1}{2\pi R_r}\sqrt{\frac{3\kappa}{\rho}\left(P_0+\frac{3\sigma}{R_r}\right)}. \qquad (5.14)$$

From curves in Fig. 5.6 it follows that if the sound pressure is small enough ($P_A < P_C$, where $P_C = 0.6$ MPA is the cavitation threshold), the cavities pulsate and do not collapse during this time. The pressure in gaseous bubbles varies very little. As the sound pressure P_A increases to values above 1 MPa and exceeds P_C, the majority of cavities with $R_0 > R_{CR}$ behave like typical cavitation bubbles, collapsing at the end of the first or second period of oscillations. With a further increase in sound pressure, i.e. for $P_A >> P_C$, cavitation becomes developed and all cavities expand during one or two periods of the ultrasound wave and then collapse. The pressure inside the bubbles varies by several orders of magnitude.

This analysis is done with an assumption of spherical bubbles, which holds only for the first cycle of oscillations. In reality the curved interface between the denser liquid and the less dense gas inside the bubble strongly accelerates inward, especially during last stages of collapse [66]. This results in the distortion of initially plane interface with the formation of

kinks and folds. This phenomenon as well as the collapse of the bubbles resulting in the formation of a cloud of new, much smaller bubbles has been observed experimentally [13, 66]. This is illustrated in Fig. 5.7. The shape instability is counteracted by the smoothing effect of surface tension and energy dissipation by viscosity [66].

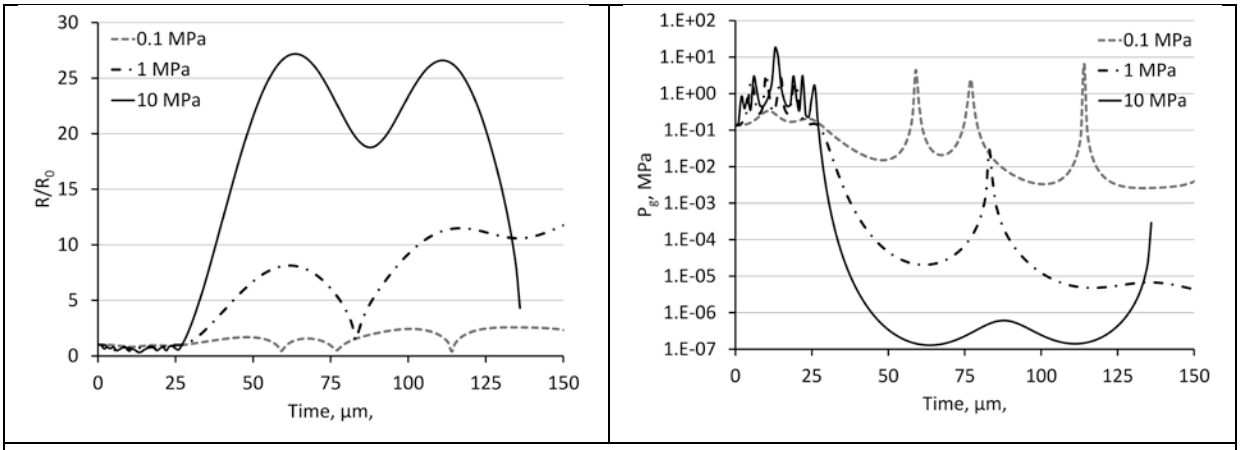

Figure 5.6. Evolution of cavities with initial radii R_0 = 50 μm in aluminum melt (a) and corresponding gas pressures (b) for acoustic pressures P_A: 0.1, 1.0, and 10.0 MPa (Courtesy of G.S.B. Lebon).

The given results for bubble dynamics, though account for the gas contents inside the bubble, did not take into account the diffusion of gas dissolved in the liquid into the cavity. Allowing for this diffusion would increase the survival chances of the bubble due to gas diffusion in melts with low saturated vapor pressure or due to vaporization from the bubble walls in liquids with high saturated vapor pressure [50].

Details of numerical solutions can be found in a review by Plesset and Prosperetti [62] and works of Fyrillas and Szeri [67], Crum [68], Lebon [69].

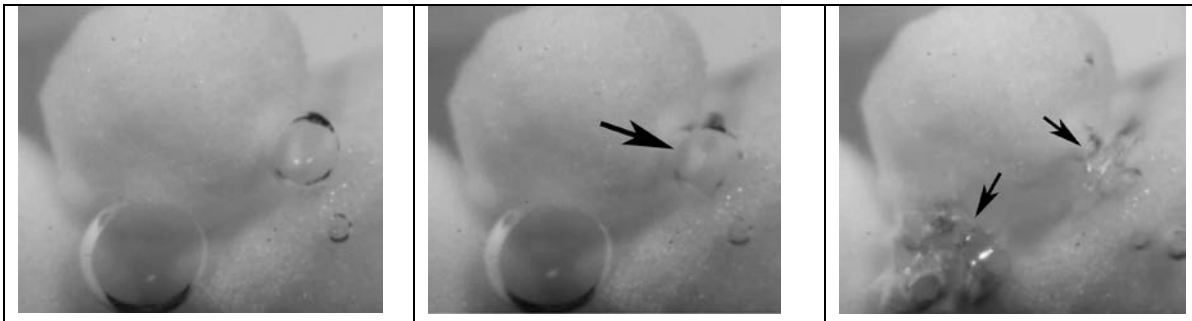

a b c

Figure 5.7. Evolution of gas bubbles in water with MgO agglomerates: (a) initial state; (b) shape distortion (shown by arrow) and (c) implosion and multiplication of bubbles (shown by

arrows). (I. Tzanakis, F. Wang, D. Eskin, 2016).

The observation of bubbles 25 μm in size in liquid aluminum performed in a synchrotron showed that the cavitation bubbles exhibited a non-linear stable behavior surviving for prolonged period of times in the melt, enhancing the broadband cavitation signal intensity and thus the cavitation treatment potential [57].

The size and geometry of the cavitation zone is not a very well-studied subject. The empirical observations show that the cavitation originates on the interfaces (radiating face of the sonotrode, walls, solid and gaseous inclusions) as well as inside the melt volume, forming a concentrated region close to the ultrasound source with complicated, changing in time configurations at a distance (Fig. 5.8). These configurations gradually transform to streams, jets and flows.

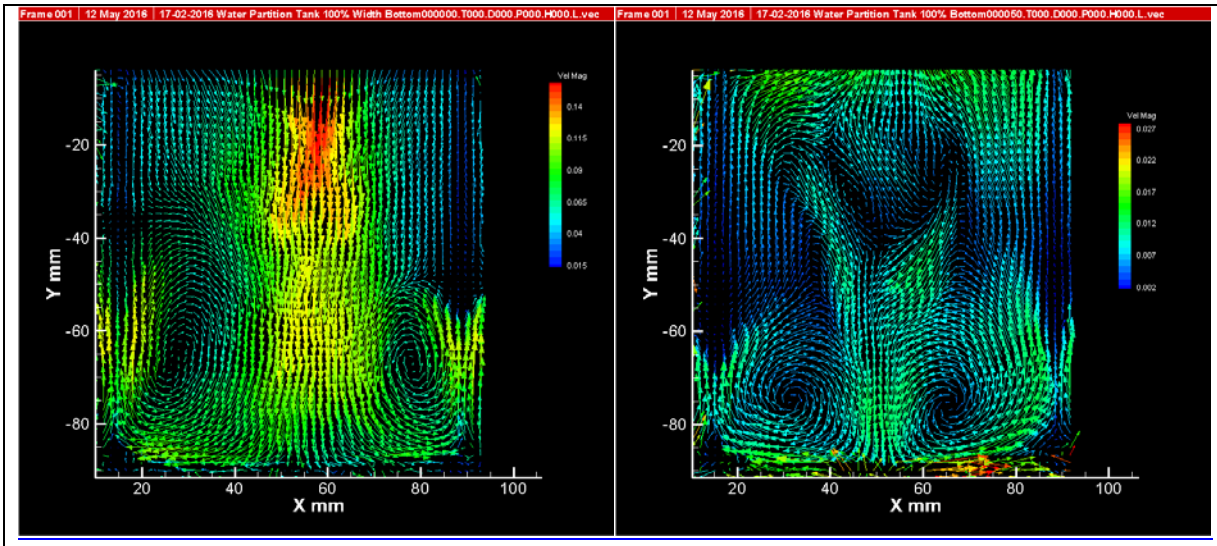

Figure 5.8. Typical velocity fields below the sonotrode tip at 100% (left) and 50% (right) transducer power settings. Legend: velocity magnitude in m/s (0.01–0.15 left, 0.01–0.03 right). The upper central part of each image is the cavitation zone. (I. Tzanakis, 2015).

The rule of thumb says that the average dimensions of the cavitation zone are on the same scale as the diameter of the sonotrode. A rough estimate of the dimensions of the cavitation zone can be obtained by direct observations, erosion of a thin foil placed under the sonotrode, or by measuring the loss of mass of special samples immersed into the liquid. When cavitation is established, the cavitation region has a volume with the cross-section

ranging approximately from $\lambda/4$ to $\lambda/2$. For example, this size is 20–40 mm for water and 50–100 mm for aluminum melts.

Figure 5.9 illustrates a typical cavitation region generated by a cylindrical horn (the type that is frequently used in metallurgical applications). There is a very densely cavitating zone close to the sonotrode (also with a specific pattern at the sonotrode face resulting from lateral distribution of wave nodes), which then develops into a cone-like structure with loose boundaries.

Figure 5.9. A typical cavitation pattern in water.

Sonication generates also directed hydrodynamic flows in melts (on the velocity scale of several cm/s). These flows are represented by (i) acoustic streams that originate from the pressure wave caused by high-frequency vibration of the sonotrode and pulsation of the cavitation region and (ii) secondary, forced convective flows. They occur both in the bulk of the liquid and near the walls, particles and other objects within the volume subjected to the ultrasonic field. The general flow pattern induced in a limited volume by an ultrasonic horn is shown in Fig. 5.10 (visualized by cavitation in viscous glycerin) [57]. A fully vortex-like structure is developed with a clear recirculating pattern as the streamlines are going back into the main streamer (see also Fig. 5.8). The origin of streams relates to the momentum acquired by the liquid when it absorbs the wave. Therefore, the velocity of acoustic streams increases with the ultrasonic intensity and the sound absorption.

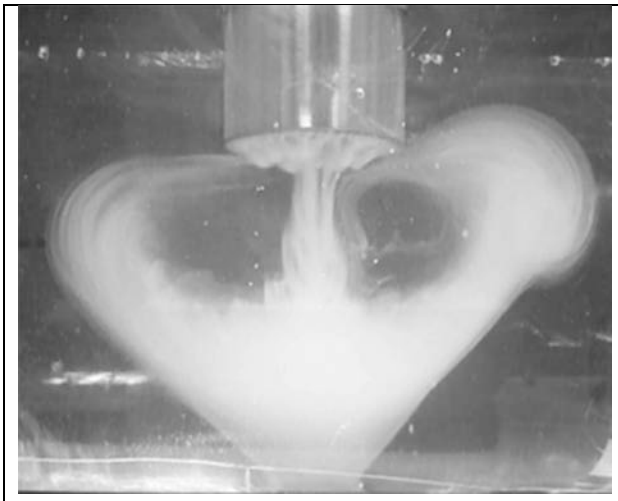

Figure 5.10. Development of acoustic streams glycerin. (I. Tzanakis, 2015).

5.3 Mechanisms of ultrasonic melt processing

5.3.1 Degassing

Boyle was probably the first to point at the potential of ultrasound to degas liquids [70]. Krüger [71] used low-power piezoceramic vibrators for degassing liquid metals, and successfully used ultrasound for degassing molten glass. As early as in 1950 Eisenreich [72] compared vacuum ultrasonic degassing with vacuum degassing and chlorine lancing. G.I. Eskin [73] demonstrated that the removal of hydrogen from liquid aluminum alloys depends greatly on the acoustic power transferred to the melt and on the development of cavitation and showed that ultrasonic degassing is more efficient than degassing with chlorine salts and by vacuum.

According to modern views, liquid metals and alloys are colloid systems, in which dispersed nonmetallic inclusions, e.g. oxides in liquid Al or Mg, serve as hydrogen concentrators as well as the cavitation nuclei. Experimental results [74] show that pure alumina and even more so alumina contaminated with transition metals adsorbs hydrogen in considerable quantities that makes these particles efficient cavitation nuclei and decreases the cavitation threshold.

The formation of single hydrogen bubbles near non-metallic inclusions determines the start of cavitation and degassing, i.e. in liquid metals the cavitation threshold coincides with the degassing threshold.

The efficiency of degassing, irrespective of physical and technical means, is a function of the concentration of dissolved gas in the liquid. This concentration is not a constant but

depends on several factors, most important of which are temperature, vapor pressure, and limit solubility.

Liquid aluminum and its alloys react with atmospheric moisture to form alumina and hydrogen. The latter actively dissolves in the melt while the former deposits at the surface. It is important to understand that the solubility of hydrogen in liquid aluminum is not a constant or a fixed number. The solubility depends on the conditions at the interface between the hydrogen-containing medium (atmosphere or bubble) and the liquid metal (surface or bulk). The quasi-equilibrium solubility exists for each combination of the hydrogen concentration in the atmosphere (humidity), in the melt (dissolved hydrogen) and the pressure (air pressure and partial pressure of hydrogen). The higher the humidity and melt temperature, the larger the quasi-equilibrium solubility of the hydrogen [75, 76].

Thermodynamic analysis [77, 78] shows that the partial pressure of hydrogen is extremely high even at low pressures of water vapor. At 727 °C and a water vapor pressure of 1.33 kPa (typical atmospheric value), the equilibrium partial pressure of hydrogen at the liquid–gas interface reaches a huge value of 8.87×10^{6} GPa, so the hydrogen content of the melt might be as high as 3.24×10^{5} cm^3/100 g. This means that all available hydrogen can be dissolved in liquid aluminum, and that relatively small atmospheric humidity may lead to high hydrogen concentration in the melt.

When, however, the hydrogen concentration reaches the quasi-equilibrium between liquid aluminum and molecular hydrogen, the dissolution stops and atomic hydrogen will have a driving force to recombine into molecules and leave the melt. As a result of these two processes, there will be a dynamic equilibrium between atomic hydrogen intake (re-gassing) and molecular hydrogen expel from the melt (de-gassing). This equilibrium can be shifted if the pressure, temperature, humidity or interface conditions change. The general possibilities for the variation of hydrogen content in liquid aluminum after ultrasonic degassing are illustrated in Fig. 5.11 [79]. It is important to note that degassing process is usually faster than the re-gassing [27].

Aluminum alloys would typically have different levels of hydrogen depending on the alloy composition: commercially pure Al will have between 0.2 and 0.3 cm^3/100 g; Al–Si and Al–Cu alloys from 0.4 to 0.5 cm^3/100 g; Al–Mg alloys between 0.4 to 0.6 cm^3/100 g. For a given charge of liquid aluminum, hydrogen content can be naturally reduced to 0.1–0.2 cm^3/100 g (degassing) giving time (up to 1 h) and typical conditions (750 °C, 30% humidity) [78, 80]. Natural degassing takes long time and is impractical for industrial applications, so different methods have been proposed for accelerating this process. Two types of degassing methods

are currently used for aluminum alloys: gas purging (rotary and lance systems) and vacuum degassing. Ultrasonic degassing has been suggested quite some time ago as an environment friendly, robust and efficient means of melt degassing [23, 50].

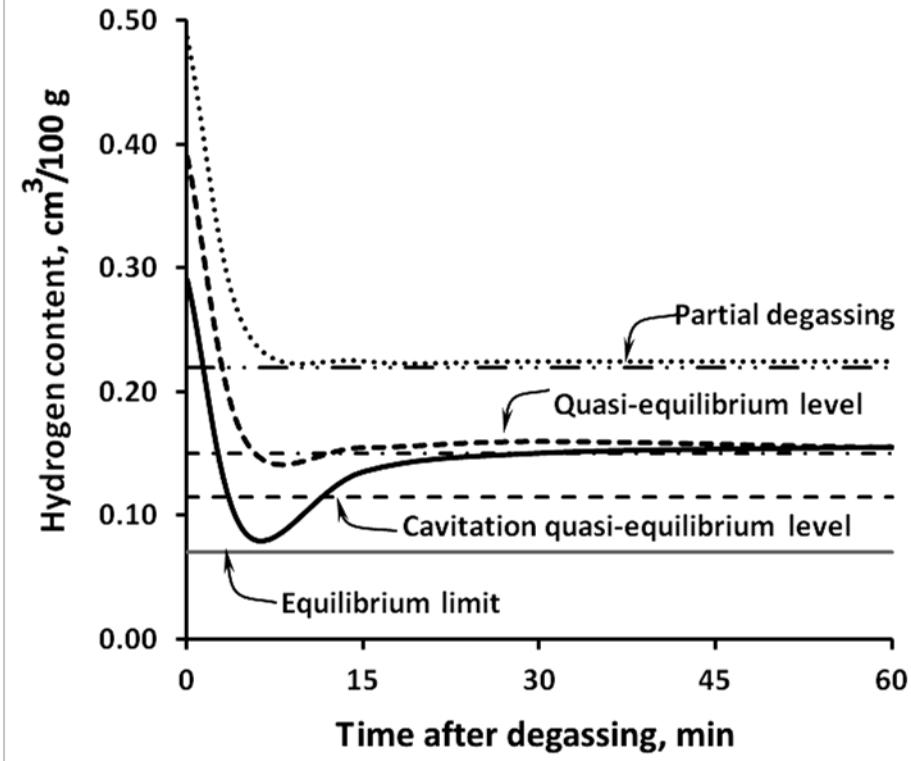

Figure 5.11. Different scenaria of degassing kinetics. (After [79])

Let us now consider the mechanisms of ultrasonic degassing of molten metal in detail. The oscillation of a bubble in the acoustic field results in rectified diffusion of dissolved gas into bubble. As a result, the gas transfer from the liquid phase into the bubble becomes possible even when the difference between the average gas concentration in the liquid C_0 and the gas concentration at the bubble/liquid interface C_g is not large. The gas concentration at the bubble interface can be written as [27]:

$$C_g = C_p(1+2\sigma/(R_0P_0)), \qquad (5.15)$$

where R_0 is the equilibrium bubble radius, P_0 is the hydrostatic pressure, and C_p is the equilibrium gas concentration in the liquid phase.

When the bubble compresses, the gas concentration inside increases and the gas diffuses to the liquid. Upon bubble expansion, the opposite process takes place. As the bubble surface (hence, interface available for diffusion) becomes larger upon expansion than that upon

compression, the diffusion rate is higher in the rarefaction stage than in the compression stage of the oscillation. Also during compression the boundary layer (where the hydrogen concentration gradient is maximum) increases in thickness while it thins during expansion. This difference in the boundary layer thickness also promotes more gas to enter the bubble during expansion than leave during compression. In other words, the oscillating bubble acts as a pump extracting gas from the liquid phase. In addition to the rectified diffusion, microscopic acoustic streams generated in the viscous boundary layer around the bubble take their part in the mass transfer, bringing fresh liquid phase to the surface of the pulsating bubble.

The actual gas solubility in the liquid phase under conditions of cavitation will be lower than the quasi-equilibrium solubility (se Fig. 5.11). There exists a limit until which the gas can be extracted from the liquid phase by cavitating bubbles. This limit was estimated to be about 50% lower than the quasi-equilibrium gas solubility under given environmental conditions. This was first established for degassing water from oxygen [27] and then confirmed for degassing aluminum from hydrogen [44, 50]. The actual value can be even smaller due to the hysteresis of gas diffusion [44]. Under conditions of cavitation the instantaneous solubility can be described as [44]:

$$C = \frac{C_0}{2} + \frac{1}{\pi}\left[\frac{C_0}{\sin(\frac{C_0}{C_A})} - C_A + \sqrt{C_A^2 - C_0^2}\right], \qquad (5.16)$$

where C_0 and C_A are the gas solubilities at the atmospheric and acoustic pressure, respectively.

The ultrasonic degassing of liquid metal is a process of three simultaneous stages [72, 27, 23, 81]: (1) gas bubbles form on cavitation nuclei and grow in the ultrasonic field accumulating hydrogen through rectified diffusion (if the liquid contains small bubbles, this stage consists only of their diffusion growth); (2) separate bubbles coalesce under the action of the Bjerknes and Bernoulli forces; and (3) bubbles float to the surface of the molten metal.

5.3.2 Wetting and sonocapillary effect

The characterization of wetting and surface tension under dynamic conditions such as under the action of ultrasonic waves and cavitation is not well developed and indirect methods are most commonly used instead. There have been however attempts to quantify the effect of ultrasonic vibrations on the wetting and surface tension using various experimental techniques adapted to dynamic conditions.

It was shown that the wetting angle of Al-Ti and Al melts on graphite decreases significantly when the ultrasonic vibrations are applied, from 150–160° before processing to 45–50° after 10 min of holding after the ultrasonication [82]. The reason behind the improved wetting is the destruction of alumina film surrounding the droplet in the case of wetting of graphite with liquid aluminum and enhanced reactive wetting by forming TiC in the case of wetting graphite with Al–Ti alloys. The improved wettability of graphite and alumina by liquid aluminum has been demonstrated in other experiments as well [83, 84]. The experiments with various low-melting alloys and metallic or ceramic substrates showed that the application of ultrasonic vibrations to the substrate results in almost immediate wetting. This effect is enhanced by increasing temperature and ultrasound amplitude. Summary of experimental results can be found elsewhere [85].

A sonocapillary effect, i.e. the penetration of liquid into thin channels assisted by cavitation, was extensively studied and the results were summarized in a monograph [86]. The crucial role of cavitation in the sonocapillary effect was proved both theoretically and experimentally [87, 88]. The liquid rise in a capillary increases by an order of magnitude under developed cavitation conditions. A sonocapillary theory [86] includes asymmetry in the boundary conditions for a collapsing cavity, when it loses its spherical shape and implodes emitting a cumulative jet of liquid. This cumulative jet is assumed to be responsible for the elevation of liquid level in the capillary. Repeated with a frequency determined by the probability of bubble occurrence and collapse near the capillary entry, the cavity collapse and jets produce accumulated liquid rise ΔH, resulting in the sonocapillary effect. In the interval between two successive jets reaching inside the capillary, the liquid can escape from the capillary and the liquid column can decrease.

The sonocapilary effect in liquid aluminum was recently confirmed by a small scale experimental study where, the re-filling of a pre-existing oxide film tube-like groove, with the action of ultrasound upon an Al-10%Cu melt was monitored using in-situ synchrotron X-ray radiography [89]. Analytical solutions of the hydrodynamic impact pressure exerted from the cavitation implosion jet and the hydrodynamic pressures required to fill the studied groove of Fig. 5.12, have shown that the mechanism responsible for the re-filling of the groove with the melt is the collapse of cavitation bubbles near by the groove inlet. Specifically, the pressure delivered by the high speed micro-jet at the inlet of the groove after the collapse of bubbles at a distance of 300 μm from that inlet is in the range of 0.3 to 46 MPa which, on the upper side, is enough to fill the groove.

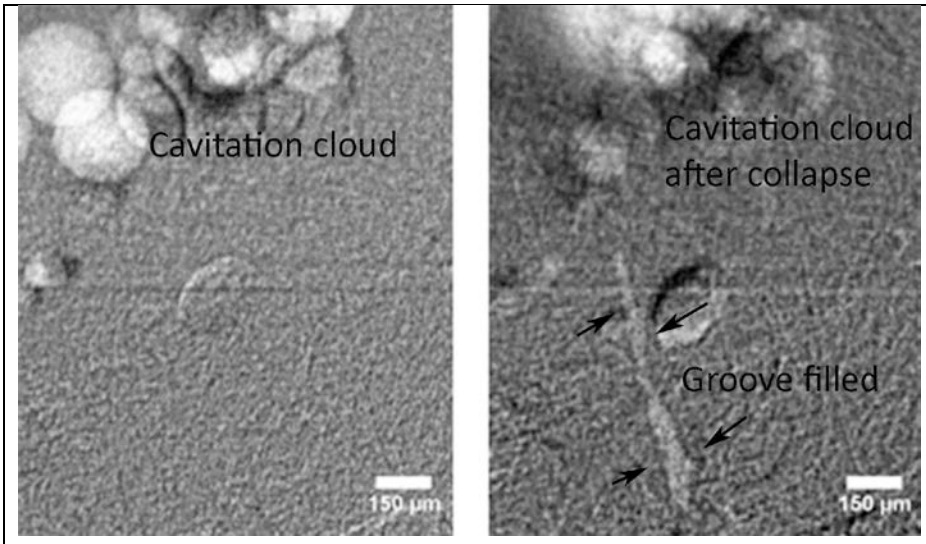

Figure 5.12. Radiographs of the pre-existing groove which (a) is not visible as it is filled by liquid melt until the moment when, after the cavitation bubbles collapse, it is refilled and revealed (b). After [89].

Additionally during the re-filling process a secondary effect was observed, related with the mass transfer of oxide particles inside the groove. The particle delivery was due to the action from the high-speed liquid micro-jet. The concentration percentage of oxide particles that are captured in the groove during melt entrainment, was quantified and found to increase with time and hence with the amount of bubble collapses events. The observed phenomenon is related to the ultrasound-assisted filtration of the melt from oxide inclusions.

Although the fundamental studies of this phenomenon are ongoing, the importance of its role in many processes and mechanisms is beyond any doubt. For a number of metallurgical procedures, such as melt degassing, filtering, wetting of solid inclusions, forming of cavitation and solidification nuclei, manufacturing of composite materials, insert casing, precision casting, the sonocapillary phenomena are essential.

5.3.3 Grain refinement

The cavitation-induced nucleation can go along the two main mechanisms (i) undercooling of the cavitation bubble surface during the expansion phase of oscillations and (ii) undercooling of the liquid phase resulted from the instantaneous increase of pressure during cavitation bubble collapse (according to the Clapeyron equation). The latter mechanism seems most probable as the decrease of bubble surface temperature does not exceed 1 K while the change of the melting point as a result of bubble collapse can reach tens of degrees and approach

$0.2T_m$ [38]. For example for 99.99% pure aluminum the increase melting temperature changes with the pressure as shown below

P, MPa	0.1	500	1000	2000	4000
t_0, °C	660.5	690.0	720.0	780.0	830.0

These mechanisms of cavitation-induced nucleation are seldom realized as they consider homogeneous nucleation, which is not a common phenomenon in real metals.

Multiplication of solidification nuclei by activation of heterogeneous substrates was suggested in the 1930–1950s by Danilov et al. [90, 91] and Kazachkovsky [92]. In this case the dynamic action upon solid/liquid interface improves wetting, decreases surface tension and promotes heterogeneous nucleation in the available insoluble substrates such as oxides, carbides etc., being assisted by penetration of the liquid phase into discontinuities of the substrate surface and the formation of the adsorbed boundary layer at the substrate surface.

Early direct observations of transparent analogues seem to confirm that nucleation is indeed facilitated by ultrasonic cavitation [23]. More recently, advances in high-speed imaging allowed for more specific observations of the interaction between cavitation and solidifying material. Swallowe et al. [93] demonstrated both nucleation of the solid phase in the ultrasonic field and fragmentation of growing dendrites by oscillating cavitation bubbles in camphene. Interesting evidence of dynamic nucleation of 15 wt% water solution of sucrose was reported by Chow et al. [94]. The nuclei were formed at a distance from the sonotrode almost immediately after an ultrasonic pulse, and they grew to equiaxed crystals.

Nucleation of primary intermetallics on alumina inclusions was demonstrated in aluminum alloys both ex-situ (Fig. 5.13a) and in-situ (Fig. 5.13b) [95, 96].

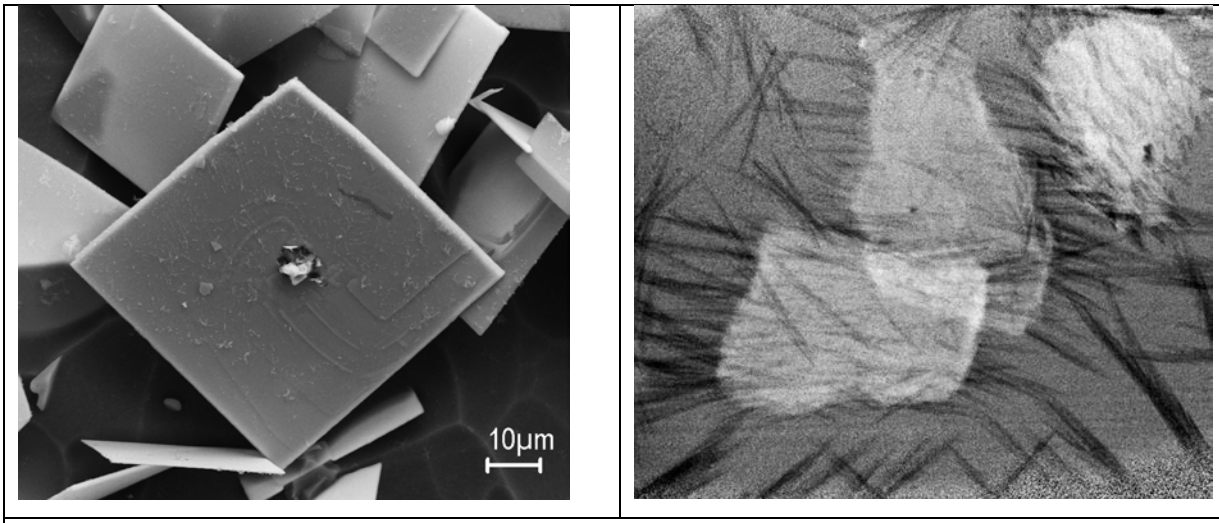

Figure 5.13. Nucleation of primary intermetallics on oxide particles after ultrasonic processing: (a) ex-situ observation of extracted Al_3Zr crystals nucleated on alumina (small particle in the center) and (b) in-situ observation in synchrotron of the formation of Al_2Cu (dark needle-shaped particles) on alumina plates. (Courtesy F. Wang).

The fragmentation of the solid phase under dynamic action is accepted by many as the main mechanism of structure refinement [19, 20, 28, 93, 97]. Chvorinov [97] suggested that the dendrites growing in the two-phase transition region are separated from the solidification front by forced convection and the resultant crystals move to the bulk of the melt and act as nuclei for new grains, providing that they are not completely re-melted. Balandin [19] enriched this idea with the thesis that the insoluble inclusions deactivated by alloy melting with high superheat reactivate once the solid phase is formed around them. After separation from the two-phase zone by forced convection, a solid crystal containing this activated inclusion is transported to the liquid phase and the solid phase is melted away leaving behind the active insoluble substrate. These concepts have not, however, explained the mechanisms of dendrite (crystal) separation from two-phase zone or its fragmentation.

One of the earliest suggested mechanisms was the seemingly obvious fragmentation of dendrites by mechanical fracture caused by melt flow. This mechanical fracture assisted by bending deformation, formation of large-angle boundaries and liquid metal embrittlement is still considered as one of the possibilities [20, 98].

On the mesoscopic scale, forced melt flow can bring hot melt from the liquid pool into the undercooled two-phase zone and cause its partial re-melting with subsequent washing-out of loose solid crystals. On the microscopic scale and in the absence of cavitation, the most realistic mechanism of fragmentation is dendrite arm separation by root re-melting effects

because of thermal, solute, or capillary effects. Solute accumulation at the solidification front causes the fluctuations in growth velocity that has direct effect on the kinetics of dendrite branches growth and coarsening [99]. The coarsening of dendrite branches results in their necking [100, 101] and accumulation of solute at their roots both by rejection from the solid phase and by convection in the interdendritic space [102]. The local solute enrichment results in local superheating of the solid phase and its melting. Along with the local change of equilibrium, capillary effects cause dendrite roots to be more soluble than other regions. The forced flow assists further by transporting the fragments to the solidification front and farther to the bulk of the liquid. The fragmentation assisted by acoustic streaming is especially applicable to elongated crystals that are subjected to alternating flow, facilitating the root re-melting and fatigue-type fracture [103].

In the presence of cavitation accompanied by the implosion of bubbles, the destruction of dendrites has been demonstrated on transparent analogues [93, 104] and recently on intermetallic crystals subjected to cavitation in water [105]. Figure 5.14 gives a sequence of frames capturing the fragmentation of primary intermetallics by an oscillating and imploding bubbles as well as a result of cavitation processing. Before fracture, oscillations of the future fragments with obvious crack propagation were observed. A fatigue-like brittle fracture mechanism was most likely responsible for the fragmentation.

The ultrasound-induced streaming flow can be effective in transporting cavitation bubbles toward the dendrites to promote continuous fragmentation of the growing dendrites, and in transporting the fragments to the bulk of the melt.

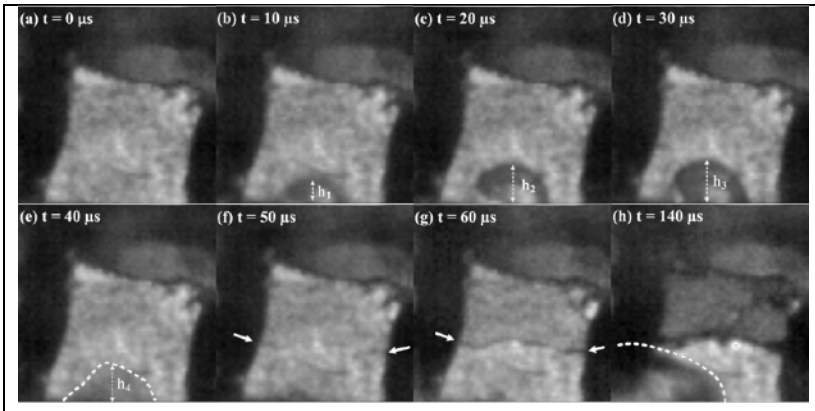

a

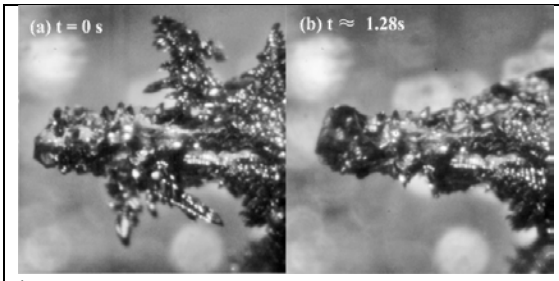

b

Figure 5.14. Fragmentation of intermetallic crystals by cavitation: (a) a sequence of images showing the fatigue crack propagation and fracture of a primary Al_3Ti crystal interacting with a pulsating cavitation bubble (a changing bubble radius is shown by *h*) and (b) fragmentation of a primary Al_3V dendrite after ultrasonic processing with input power 200 W in distilled water for around 1.28 s [105].

Solidification of real melt always occurs heterogeneously and on available substrates that are either naturally present (indigenous impurities) or deliberately added (exogenesous, grain refiners) to the melt. In aluminum and magnesium alloys the former are represented by oxides and carbides and the latter by borides, carbides and primary phases. The term "activation" is usually applied to indigenous particles and includes the phenomena of wetting, formation of stable or metastable surface layers, deagglomeration, and nonequilibrium solidification.

Let us look closer at the particles that can be activated and involved in solidification in light alloys.

The activation of inclusions by ultrasonic cavitation has been demonstrated for pure aluminum with mixed in oxide surface film [106] and for Mg–Al alloys with added carbon black nanoparticles [107]. Recently an ultrasonic activation of spinel particles (potent substrates for aluminum) from an Al–1.3% Ti–1.8% $MgAl_2O_4$ master alloy added to an aluminum casting alloy has been demonstrated as shown in Fig. 5.15 [108].

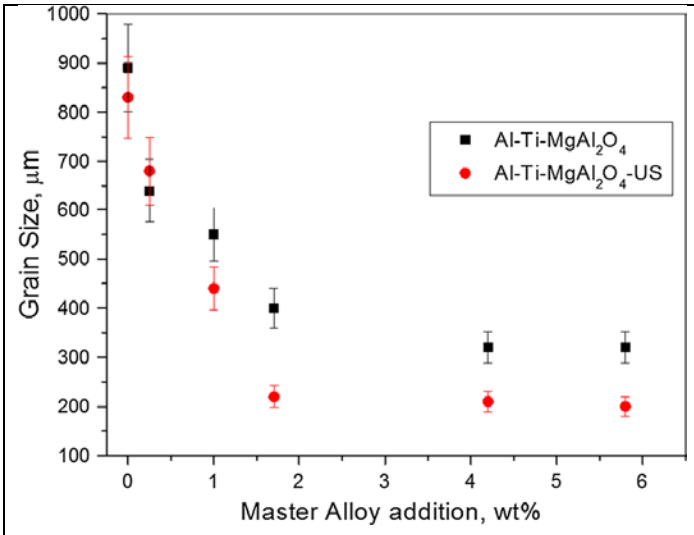

Figure 5.15. Relation between grain size of A357 and the level of Al-Ti-MgAl2O4 master alloy addition with and without ultrasonic processing (adapted from [108]).

Cavitation treatment may turn particles into active solidification sites by the following mechanism [50].

Any microscopic solid particle that has affinity to the solidifying phase has a potential to become an active solidification site. This affinity can be due to the match of crystal structures, or due to the presence of a special adsorbed layer or even the matrix solid phase on its surface. In the latter case, the stability of such a solidification site can be assured only when the adsorbed layer or the solid phase is thermally stable within some temperature range above the liquidus of the alloy. Such conditions can be met in discontinuities like microcracks where, due to the capillary effect, the melting temperature of the alloy is much higher than the equilibrium liquidus. The increase in the melting point under conditions of negative curvature (concave particle) is described by the Gibbs–Thompson equation [109]:

$$T_{\mathrm{m}}^{\mathrm{r}} = T_{\mathrm{m}}^{\infty} - \frac{2\Gamma}{r}, \qquad (5.17)$$

where $T_{\mathrm{m}}^{\mathrm{r}}$ is the melting point of a concave particle inside a crevice, T_{m}^{∞} is the melting point of a particle with flat interface; r is the curvature (negative in the case of the concave particle) and Γ is the Gibbs–Thompson coefficient depending on the surface tension, density and latent heat.

However, the presence of a gaseous phase at the surface and in the surface imperfections of non-metallic particles hinders the access of the liquid phase to the inclusion, wetting and filling of the imperfections with the melt. Therefore, the majority of the inclusions remain inert with regard to the solidification.

During ultrasonic treatment with intensity higher than the cavitation threshold, a cavitation bubble is formed close to the capillary opening filled with gas. In this place the cavitation strength of the melt is weakened by the presence of a gaseous phase. Then the sonocapillary effects takes over, filling the capillaries of almost submicroscopic sizes (see section 5.3.2). At the same time, the particle is stripped of absorbed gas and becomes accessible by the surrounding melt. As a result of this activation, the solidified alloy inside capillary openings (cracks) of the particle stays solid at a temperature of the surrounding melt and acts as a perfect solidification site for the matrix melt. The same mechanism should be valid for any primary solidifying phase; solid solution, intermetallic, or silicon. Actually, the activation of nonmetallic impurities facilitates nucleation and refinement of any primary phase as shown in Fig. 5.13.

A comparison between ingots from a high-strength aluminum alloy produced with and without ultrasonic cavitation treatment during DC casting shows that the number of active nuclei increases by several orders of magnitude after the cavitation treatment (Fig. 5.16). For example, the cavitation treatment in the case of small-sized ingots (65–74 mm) enables the activation of nucleation substrates with the density up to 10^9 per cm^3 as compared to 10^3 per cm^3 without sonication. In the case of middle-sized ingots (270–285 mm), this difference reduces to four orders of magnitude; for large-sized ingots (830–845 mm), this difference reaches three orders of magnitude.

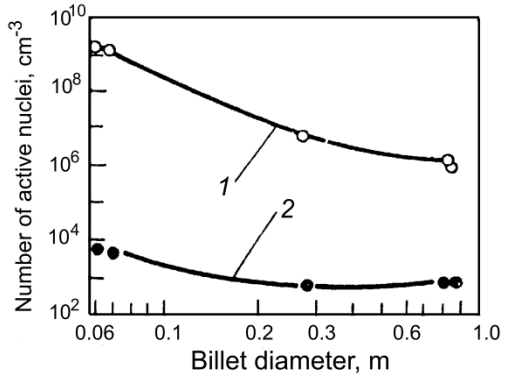

Figure 5.16. A change in a number of active nuclei upon solidification of a direct-chill cast billets from a 7XXX-series (Al-Zn-Mg-Cu-Zr) alloy with ultrasonic melt processing (1, without ultrasonic processing and 2, with ultrasonic processing) (adapted from [84]).

De-agglomeration and dispersion of nucleating particles is another mechanism of grain refinement. The high-intensity ultrasonic oscillations create vast number of microscopic bubbles that are distributed within the volume by acoustic and secondary flows. The bubbles

preferentially form at the interfaces and gas pockets. Therefore the agglomerates of the particles and particles themselves are ideal nuclei for cavitation. The mechanisms of de-agglomeration can be represented as follows: the cavitation bubbles are formed at the interfaces particle/gas pocket/liquid. These bubbles pulsate intensely, implode, loosening the agglomerate and chipping off particles. The local pressure generated (up to 500 MPa) far exceeds the forces that hold together the particles in agglomerates, i.e. up to 1 MPa (capillary and adhesive forces) [110, 111]. The acoustic flows generated by the cavitation zone, distribute the particles further in the volume.

Some practically important analytical calculations show (thought semi-quantitatively due to the assumptions) the dependence of processing time on the surplus in pressure at the capillary entry (difference between the capillary pressure and the pressure from cavitation) and relative sizes of capillary channels (depth/radius) as illustrated in Fig. 5.17a as well as the requirement for the minimum acoustic pressure at the entry to the capillary in dependence on the agglomerate size and processing frequency in Fig. 5.17b [112]. It is important to make two notes: (i) the deagglomeration is not an instantaneous process but takes time and (ii) the ultrasonic frequency is preferable over sonic frequencies.

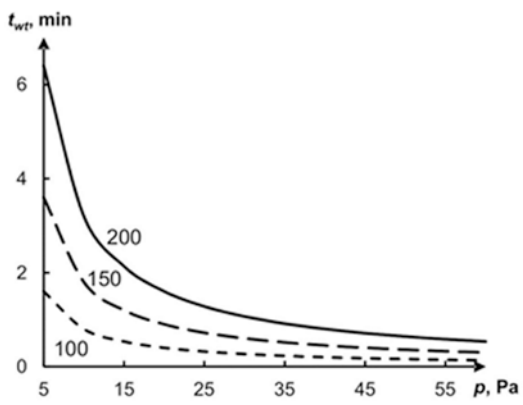

a

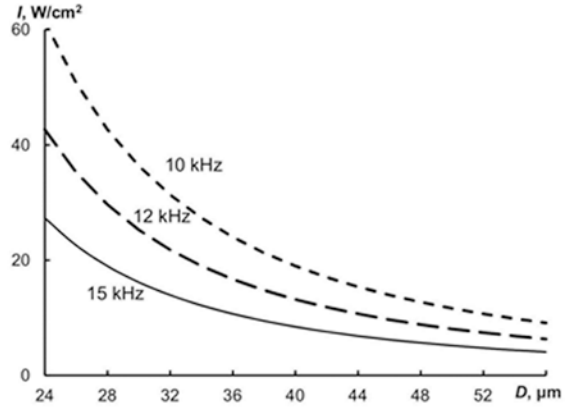

b

Figure 5.17. (a) The dependence of the processing time required for liquid penetration into an agglomerate on (a) the surplus pressure at the entry to a capillary channel (numbers show the relative size of the channel, i.e. depth/radius) and (b) dependence of the threshold (ultra)sound intensity for break-up of agglomerates in liquid aluminum on the particle diameter for various values of the sound frequency (after [112]).

Grain refinement can be achieved by additions of elements that form primary intermetallics with good crystallographic match with the matrix solid solution, i.e. aluminum or magnesium. In aluminum alloys, titanium aluminide and scandium aluminide are well

known to possess structural features required for powerful grain refinement effect; in magnesium alloys – zirconium forms a primary phase that is used in Al-free alloys for grain refinement.

It has been known since the 1960s that the addition of Zr in combination with ultrasonic treatment results in considerable grain refinement of aluminum alloys [23]. Later on the essential role of small Ti additions has been demonstrated [50] and the combined effect of Zr, Ti and ultrasonic processing has been explained [113, 114]. The fragmentation of primary intermetallic particles by cavitation is one of the mechanisms for grain refinement of the main primary phase, e.g. Al. Fracture by oscillating and collapsing bubbles can happen to the primary intermetallics in the range of their formation, in addition to the enhanced nucleation of insoluble inclusions [115, 116]. In this case the alloy would be considered liquid from technological point of view as the formation of these particles as well as the ultrasonic processing occur well above the liquidus temperature of the matrix solid solution.

The fragmentation of dendrites can also result in spectacular structure refinement, when ultrasonic processing happens in the solidification range of the matrix [117]. Despite very good grain refining effect of fragmentation, the practical application of this mechanism is limited to small volumes. There might a potential to use this mechanism in direct-chill casting or other continuous processes (e.g. arc re-melting) where the position of the solidification front is fixed in space and the cavitation can be applied throughout the process in the locations below the liquidus isotherm. The limitation in this case would be lateral spread of the effect, i.e. multiple cavitation sources would be required for processing of larger cross-sections.

5.3.4 Emulsification (Immiscible Alloys)

The emulsification of immiscible liquids under the action of ultrasound is known since the 1920s and was demonstrated for water and oil and water and mercury [118, 119]. The decisive role of cavitation in the process of emulsification was soon recognized [120]. Already in the 1930s first successful experiments on ultrasonic (10 kHz) introduction of Pb in liquid Al and Cd in Al–Si melt were reported [32] and the possibility to produce emulsions of 7–10% Pb in Al and Zn stable even upon re-melting was demonstrated [45].

The physics of ultrasonic emulsification is considered elsewhere [121, 122, 123, 124, 125]. Some basic factors controlling the process can be summarized as follows. The size of droplets in the emulsion decreases with the increasing ultrasonic frequency. At the same time

the higher intensity requires a greater sound intensity applied. With the increasing intensity and processing time the emulsion concentration increases up to a certain value when saturation occurs. This saturation is a result of the equilibrium reached between the processes of emulsification (dispersion) and coagulation. A running sound wave is more efficient than a standing wave, with coagulation processes prevailing in the latter case. Pre-cavitation sound processing results in de-emulsification. Therefore, cavitation is the important requirement of the process. A low viscosity and a lesser difference in viscosities between the components facilitate emulsification. Additions of surfactants (decreasing the surface tension at the interface) and stabilizers (coating of droplet surface) promote the stability of the emulsion and allows for higher concentrations. In general the emulsification occurs through local disturbances at the interface between two immiscible liquids with typically only one liquid undergoing dispersion while the other liquid acts as the source of cavitation bubbles. The disturbance occurs during the expansion phase of the bubble oscillation, while the dispersion happens upon bubble collapse. Figure 5.18 illustrates the formation of a wave disturbance in liquid B caused by an expanding bubble in liquid A. When this bubble starts to contract it draws the crest of the wave of liquid B upwards, this crest extends with acceleration following the accelerated contraction of the bubble. When bubble collapses, the crest disintegrates forming a droplet.

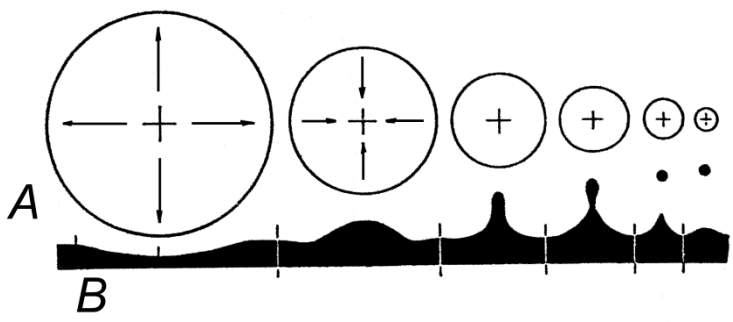

Figure 5.18. A diagram illustrating the mechanisms of ultrasonic emulsification.

With respect to liquid metals and alloys, ultrasonic emulsification has practical value for manufacturing of free-machining and bearing alloys. These alloys contain additions of low-melting, soft elements such as Pb, Bi, Sn that have either a miscibility gap with Al that causes stratification (Al–Pb, Al–Bi) or a very large solidification range that triggers gravity segregation (Al–Sn).

It was demonstrated that application ultrasonic cavitation significantly decreases macrosegregation and promotes the uniformity of structure in an immiscible Al–Sn–Cu alloy.

With a single ultrasonic source the uniform distribution of monotectic Al–Sn–Al_2Cu cells was obtained close to the cavitation region, while non-uniformity triggered by gravity separation of Sn from Al remained in the areas farther from the ultrasonic source where only acoustic streaming was acting [126]. It was also observed that the monotectic cells nucleate on cavitation-affected substrates. An innovative scheme of ultrasonic processing with three orthogonal sources was developed and applied to the solidification of a similar immiscible alloy [127]. In this case the homogeneous monotectic structure was obtained in the entire 30×30×100 mm volume, due to the uniform cavitation field created in the melt.

5.4 Practical implementations of ultrasonic melt processing

5.4.1 Degassing

The ultrasonic degassing of aluminum was implemented in foundries for precision investment, sand, gravity, low-pressure and high-pressure die casting [23]. Let us look at the example of sand casting. A special ultrasonic degassing system UZD-200 has been developed in 1959 for degassing up to 250 kg of melt in stationary volume (Fig. 5.1). The installation (in stationary and mobile versions) consisted of a 10 kW generator that fed 4 magnetostrictive transducers that worked in a sequence with a time gap of 15–20 s. The frequency was 19.5 kHz and the total acoustic power – 1.6 kW. Table 5.1 summarizes these results for castings of an A361.1 alloy. It can be easily seen that, ultrasonic degassing significantly increases the density of cast metal and makes it possible to obtain almost pore-free castings (rank 1 in the porosity scale).

Table 5.1. Comparison of various degassing methods for an A361.1 alloy [84].

Degassing method	H_2 content $cm^3/100$ g	Density g/cm^3	Porosity rank	Tensile properties	
				UTS, MPa	El, %
Starting melt	0.35	2.660	4	200	3.8
Ultrasonic degassing	0.17	2.706	1–2	245	5.1
Vacuum treatment	0.2	2.681	1–2	228	4.2

Argon blasting	0.26	2.667	2–3	233	4.0
Hexachloroethane	0.3	2.665	2–3	212	4.5

In recent years a design that includes a moving sonotrode has been tested for degassing of up to 500 kg of aluminum melt [128]. This principle is based on the idea that the degassing involves (as we have discussed in Section 5.3.1) three stages: generation, growth and flotation of the bubbles. When the sonotrode is moving through the volume it generates bubbles in the volume part, then moves to the next part to cause cavitation there, while the bubbles in its wake grow in the sound field (that covers much larger volume than the cavitation zone) and float to the surface. One moving sonotrode, therefore, effectively substitutes for several stationary ones. The degassing performance was shown to be very similar to the commercial Ar-rotary degassing with 4-5 times less dross formed at the melt surface. Figure 5.19 shows the degassing prototype based on a robotic arm, magnetostrictive transducer and Nb sonotrode.

Figure 5.19. Ultrasonic degassing machine with a moving ultrasonic source in the process of degassing 500 kg of a liquid aluminum alloy (courtesy J. Tort Guzman, Doshormat, FP7 project No.606090).

The requirement for processing of large, industrial-scale volumes of melt, especially in large foundries and continuous casting plants shows a limit for batch degassing operations. Another approach needs to be used and the processing of the melt flow seems like a logical and viable possibility. In large melting/casting operations, it is more appropriate to relocate

the cleaning of melts from gaseous and oxide inclusions from the melting or holding furnace to the zone of metal transfer, somewhere en route from the furnace to the mold.

First industrial trials on ultrasonic degassing in melt flow were performed in USSR in the early 1960s during DC casting of aluminum alloys using a setup similar to that described above for the batch ultrasonic degassing (UZD-200) (Fig. 5.1). The difference was in the arrangement of sonotrodes, they were put in line [129]. With taking into account that DC casting involves high flow rates and relatively low melt temperatures, a principle of multiple ultrasonic processing of melt flow was used. The launder contained a section of ultrasonic processing and a section of gas release. The melt flow rate was about 70 kg/min and the ultrasonic intensity about 5 W/cm^2. The results demonstrated that the ultrasonic degassing in the melt flow allowed for a 1.5–2 times decreased hydrogen concentration in the melt, as demonstrated in Table 5.2. One can notice that the efficiency of degassing commercially pure aluminum is less than for more concentrated alloys. This might be a consequence of its higher purity in solid inclusions with corresponding lesser cavitation development. The amount of defects (porosity, nonmetallic inclusions) decreased by a factor of 5–8, e.g. from 0.82 to 0.1 mm/cm^2 in a 460-mm billet of a AA2038-type. The mechanical properties were also improved.

Table 5.2. Concentration of hydrogen before and after ultrasonic degassing upon DC casting of aluminum alloys [84].

Alloy type	Ingot/bullet size, mm	Casting speed, mm/min	Hydrogen concentration, cm^3/100 g	
			No degassing	Ultrasonic degassing
AA1030	1040×300	123	0.28	0.18
AA2024	1480×210	123	0.41	0.24
AA2117	460 dia	35	0.4	0.21
AA1070	350 dia	44	0.2	0.10
AA5017	350 dia	65	0.42	0.3

This experience was later extended to DC casting of various aluminum alloys including Al–Mg (2 to 6% Mg), Al–Zn–Mg–Cu (AA7055-type), and Al–Cu–Mg (AA2038 and

AA2214-type). The number of ultrasonic sources were varied depending on the ingot cross-section, melt flow rate and the desired degree of degassing.

Industrial-scale degassing plant was designed and manufactured for casting large flat ingots (1700×300 mm) from an AMg6 Russian Grade (6% Mg, 0.6% Mn). The degassing was performed in a specially designed section of a launder at 20 m from a 40-tonne holding furnace. The melt flow rate was up to 100 kg/min. Each of four to twelve 4.5-kW magnetostrictive transducers was delivering up to 1 kW of acoustic power into the melt. Two schemes of ultrasound input were tried, from the bottom of the launder and from the top of the melt [130]. The latter version proved to be more reliable and efficient.

The efficiency of ultrasonic degassing with regard to the acoustic power introduced to the melt, other acoustic parameters and the dimensions of the ingot/biller is given in Tables 5.3 and 5.4. The efficiency of this process shows a distinct dependence on the metal flow rate and acoustic power (or the number of sources) conveyed to the melt [50].

Table 5.3. Hydrogen content (H_2) and relative porosity (*P*) in flat 1700×300-mm ingots of an AMg6 alloy for various acoustic powers used in ultrasonic degassing in the melt flow during DC casting [84].

Acoustic power, kW	H_2 in melt, cm^3/100 g		Ingot properties			
			No degassing		Ultrasonic degassing	
	No degassing	US degassing	H_2 in solid, cm^3/100g	*P*, %	H_2 in solid, cm^3/100g	*P*, %
4	0.60	0.45	0.41	n/a	0.36	n/a
5	0.60	0.42	0.44	0.6	0.35	0.51
7	0.58	0.39	0.41	0.66	0.33	0.55
11	0.56	0.29	0.38	0.56	0.20	0.40

Table 5.4. Efficiency of the ultrasonic in-flow degassing of an AMg6 alloy in relation to the billet diameter, and the number and intensity (*A* is the oscillation amplitude, *W* is the input acoustic power density) of ultrasonic sources with a 40-mm diameter radiating face [84].

Billet diam.,	Number	Ultrasonic	Hydrogen content*	Degassing

mm	of sources	parameters		cm^3/100g		efficiency
		A, μm	*I*, W/cm^2	initial	final	%
127	1	15	30	0.4	0.25	37
204	1	5	3	0.67	0.46	25
204	1	10	15	0.67	0.39	40
204	1	20	60	0.67	0.28	58
370	1	12	40	0.31	0.26	13
370	2	20	60	0.48	0.24	50
370	3	20	50	0.51	0.19	60

*Data obtained by vacuum extraction from the billet.

Despite these successful industrial applications, the further development and spreading of this experience was hindered by the bulkiness of the equipment and lack of optimization of melt flow. Current efforts are concentrated on understanding the interaction between the melt flow, cavitation field and acoustic streaming via physical and numerical modeling. Also new schemes of ultrasonic processing in the melt flow are under scrutiny.

One of the possible schemes involves using a plate sonotrode placed at the bottom of a launder [131]. This allowed the similar degassing efficiency in the flow as could be achieved in the stationary volume with a conventional cylindrical sonotrode as illustrated in Table 5.5.

Table 5.5. Results of ultrasonic degassing in batch and continuous operation using different schemes of ultrasonication [131].

Degassing method	Density index before degassing, %	Density index after degassing, %	H_2, cm^3/100 g before degassing	H_2, cm^3/100 g after degassing	Degassing efficiency, %
Natural	15.7	16.3	0.22	0.23	-4.5
Cylindrical sonotrode (Batch)	20.3	14.7	0.36	0.195	46
Plate sonotrode (Batch)	22.45	9.24	0.44	0.11	75
Plate sonotrode (Flow)	22.9	15.5	0.46	0.21	54

Another suggestions are to combine the ultrasonic degassing with Ar lancing in a vessel through which the melt is constantly flowing [132] or using a hollow sonotrode through which a carrier gas is supplied to the melt [133].

5.4.2 Grain refinement during casting

DC casting on one hand simplifies the application of ultrasonic melt treatment as the melt containers (launder, mold, melt distribution systems) are simple and constant in shape with well-defined temperature profiles. On the other hand, DC casting requires processing of larger melt volumes in a continuous manner, which creates some challenges for the technology of ultrasonic processing.

The first industrial DC casting installation with ultrasonic melt processing (USP) was built in the 1970s at one of Soviet metallurgical plants. A standard DC caster with a 10-t holding furnace was equipped with an ultrasonic processing station that could be controlled remotely. The ultrasonic processing was performed by dipping several sonotrodes (each fed by an individual water-cooled 4.5 kW transducer) into the sump of a billet or an ingot. The horns were made of a Nb-alloy that assured the stable and continuous operation in the melt during the entire casting process. The choice of Nb alloys as the most suitable material for ultrasonic horns for liquid aluminum processing was proven in the 1960s [23].

The main casting parameters of DC casting with ultrasonic melt processing are given in Table 5.6 [84]. Depending on the size of the billets, one to ten transducers with sonotrodes placed into the sump of the billet were used in a single casting in order to achieve uniform nondendritic structure in the entire billet.

It was possible to refine grains substantially, especially in aluminum alloys containing Zr and Ti. In some cases, a uniform structure with nondendritic grains were obtained for billets 74 to 1200 mm in diameter, respectively. Figure 5.20 gives some examples. Billets and ingots with such a structure exhibit higher mechanical properties, improved casting properties, better response to heat treatment and deformation [50, 84]. Fine equiaxed grains were also characterized by reduced microsegregation and finer non-equilibrium eutectic particles, which resulted in shorter homogenization times.

Table 5.6. Main processing parameters for DC casting of round billets with ultrasonic melt processing in the sump [50].

Billet diameter, mm	Casting speed, mm/min	Acoustic power, kW*
70–100	180–240	0.6–0.8
100–200	90–180	0.8–1.0
200–300	36–90	1.0
300–400	24–36	1.0–3.0
400–500	18–24	3.0–7.0
600–1200	12–18	7.0–10.0

* The maximum acoustic power produced by a single 18-kHz source used is 0.6–1.0 kW.

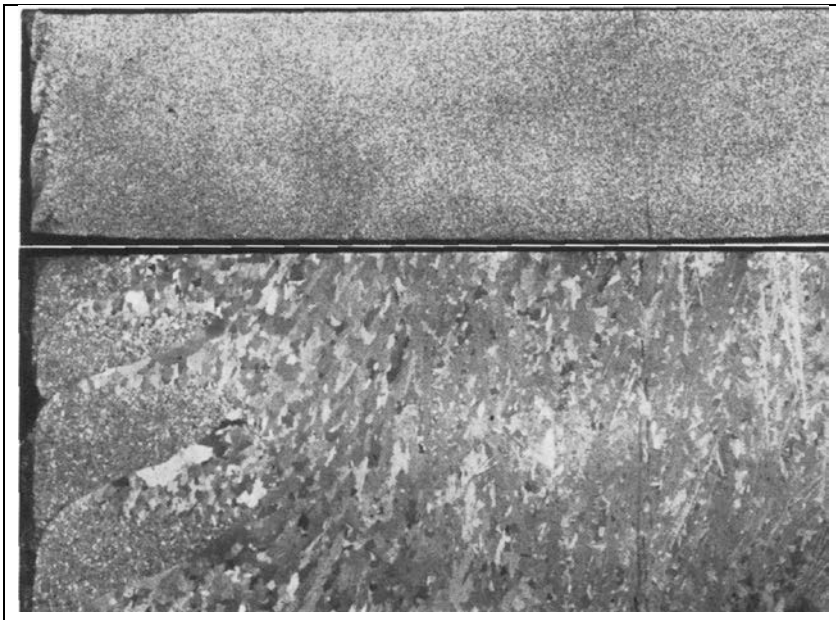

a

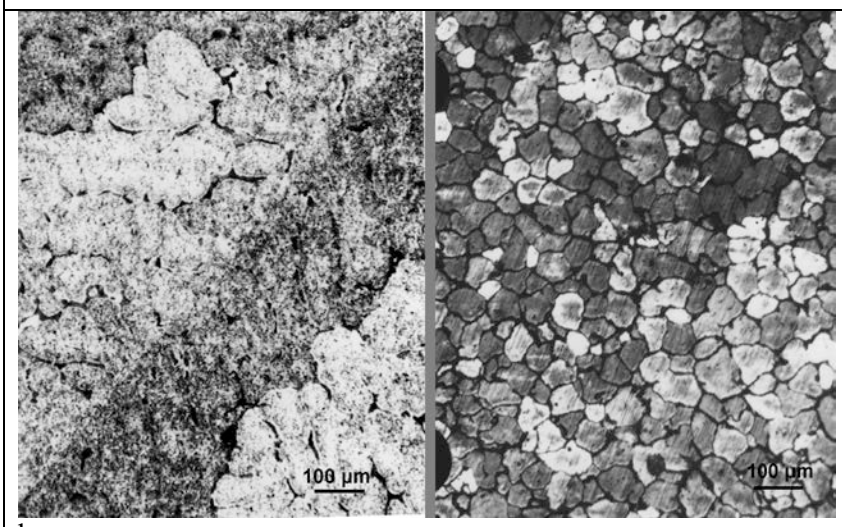

b

Figure 5.20. Effect of ultrasonic melt processing in the billet sump on the grain structure of (a) 830-mm billet from an AA7474 alloy (top – with USP, bottom – without USP) and (b)

285-mm billet from an AA7055 alloy (left – without USP, right – with USP). (Courtesy G.I. Eskin).

The uniformity in structure and chemical composition translates in the uniformity and high level of mechanical properties. As a consequence the susceptibility of the cast metal to hot and cold cracks decreases. It is well known that higher ductility of semi-solid and solid metals plays decisive role in the occurrence of hot and cold cracks, respectively [134,135, 136, 137]. In the solid state, the ductility at temperatures below 300 °C should be larger than 1.0% in order to prevent cold cracks (as the cast metal is subjected to tensile strains in an order of 0.55–0.6% [138]). Nondendritic structure assures that the ductility stays above 2% that guarantees crack-free billets.

Large deformed items for aircrafts made from high-strength alloys require high characteristics of fracture toughness and fatigue endurance. These requirements are typically met by increasing the purity of the alloys with regard to Fe and Si. This, however, results in coarsening of the grain structure and higher susceptibility to cracking upon and after casting. Ultrasonic melt processing and the formation of nondendritic structure in larger billets and ingots made it possible to meet the challenge and solve the problem of producing large castings without cracking and with uniform fine structure [50, 78, 139, 140, 141, 142]. As a result of gained experience in industrial DC casting with ultrasonic melt processing of various alloys and different-scale billets, it became possible in the 1980s to commercially produce large-scale crack-free billets 960 mm (AA7055) and 1200 mm (AA2324) in diameter. These billets were used for special forgings and extrusions for transport airplanes [143, 144]. This experience was extended to flat ingots of an AA2324 alloy where the nondendritic structure was successfully obtained in ingots 450×1200 mm in cross section. The ultrasonic melt processing can be applied to the melt flow, during the transport of the melt from the holding durance to the mold. This technological way is more versatile as the processed melt can be directed to several molds but also poses as number of challenges related to the treatment time–melt volume–acoustic power ratios. The grain refinement can be achieved in by ultrasonic melt treatment in the flow [84] but its efficiency for grain refinement is less that for processing in the mold. In this case, the mechanisms of substrate activation and refinement of primary particles are acting. The efficiency may be improved by managing the melt flow by dams and baffles.

Figure 5.21 shows the grains refinement achieved in a 85-mm billet after the melt was treated in different ways [145]. In this case the comparison is made between a 6XXX-series

alloy with a commercial AlTiB grain refiner addition (a), the same alloy containing small additions of Zr and Ti cast without USP (b), the same alloy with USP either in the melt outside the DC casting mold (c) or in the sump of the billet (d). It is clear that the USP results in a significant grain refinement as comparison with a commercial grain refiner, and that the processing in the sump gibes smaller grains than the processing outside the mold. This difference is most likely due to the action of the additional refining mechanisms, i.e. dendrite fragmentation.

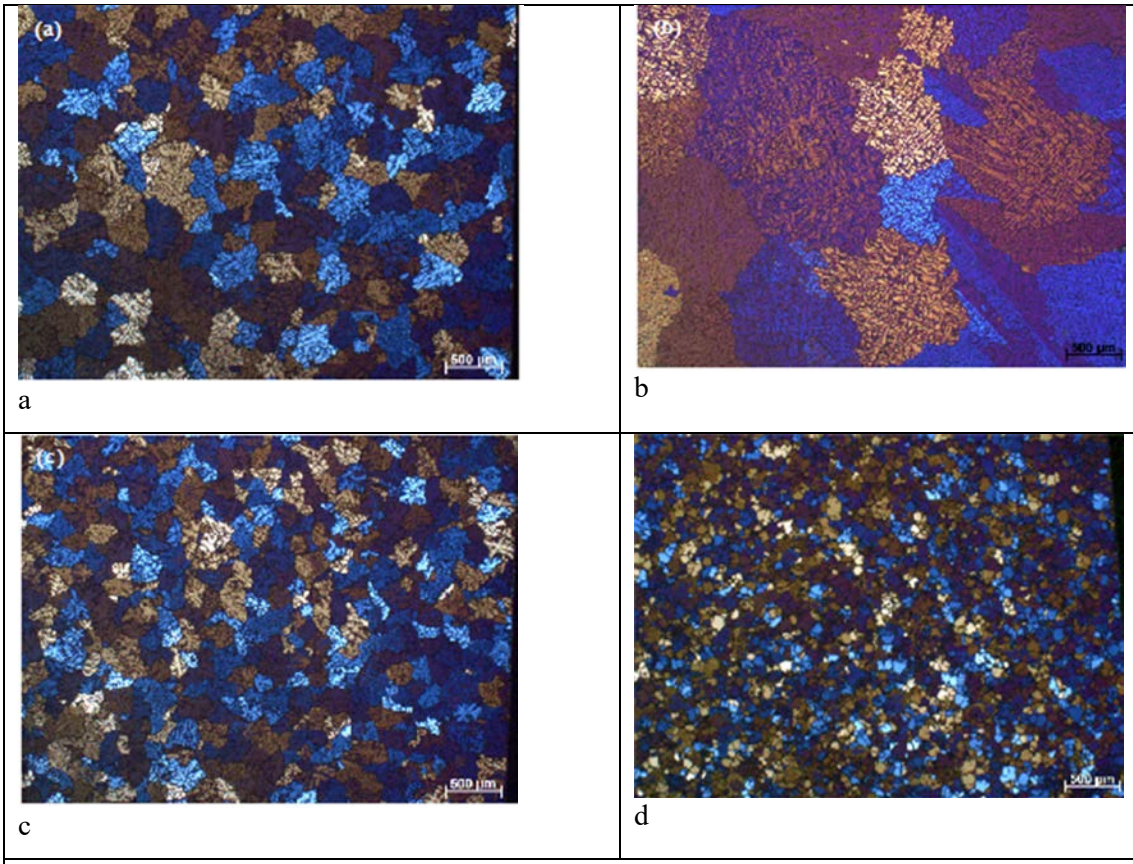

Figure 5.21. Grain structure of an AA6XXX-series alloy direct-chill cast in a 85-mm billet: (a) with standard AlTiB grain refiner, No USP; (b) with Zr+Ti addition, no USP; (c) with Zr+Ti addition, USP outside the mold; and (d) with Zr+Ti addition, USP in the sump. (Courtesy G. Salloum-Abou-Jaoude).

Grain refining additions of Zr and Ti can be added to the melt using an Al–Zr-Ti master alloy with simultaneous ultrasonic melt processing [146].

The application of ultrasonic cavitation to introduction of grain refining master alloys is very promising. The introduction of an Al–Ti–B grain refining rod was suggested in the 1970s [147] but was widely adopted later in the 1980s [148]. One of the deficiencies of grain-refining rod introduction is the agglomeration of TiB_2 particles, wide size distribution of these particles and, as a consequence,

low efficiency, i.e. only several percent of particles are acting as nucleation substrates [148, 149]. Ultrasonic melt processing improves the performance of standard AlTiB master alloys by dispersing agglomerates and activating substrates as has been confirmed by a number of studies [111, 150, 151]. Figure 5.22 illustrates this by an example of AlTiB introduction into Al–Si alloys that usually show grain coarsening at higher concentrations of Si.

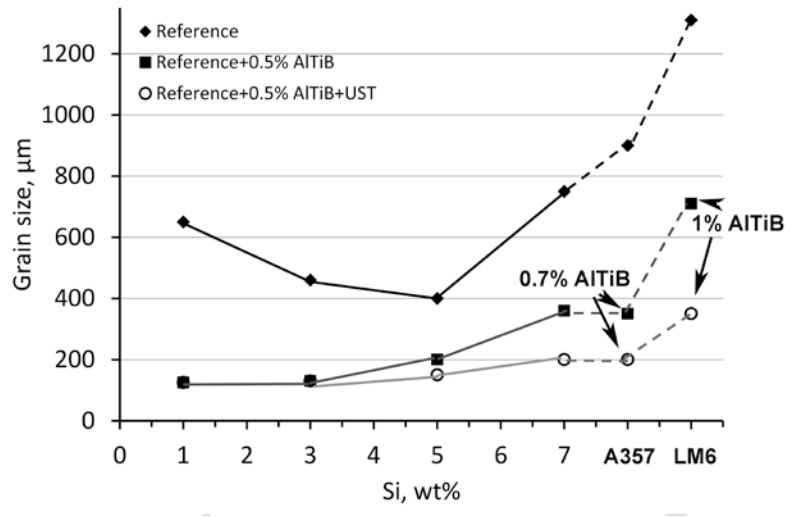

Figure 5.22. Effect of a commercial AlTiB grain refiner and ultrasonic treatment (UST) on the grain size in binary and commercial Al–SI alloys.

5.4.3 Composite materials and immiscible alloys

Ultrasonic cavitation and streaming are widely used for making metal-matrix composite materials through a liquid-metal route, for composites with nanoparticles this is a main technique used nowadays. The mechanisms of ultrasonic processing such as wetting, deagglomeration and dispersion are used.

The simplest technique of introducing the particles is spraying them onto the surface of the melt using a trough or a tube. These particles are then drawn into the bulk of the melt by vortex (in the case of impeller) or by gravity and surface flows [152, 153, 154, 155]. This technique works quite well in magnesium MMCs but have limitations in aluminum MMCs due to the strong oxide film at the melt surface. A combination of the impeller and protective atmosphere are required.

Particles can be also wrapped in a metallic foil (e.g. in aluminum foil for Al MMCs) to form a sort of a compact rod that is then slowly fed into the cavitation region, where the foil

dissolves releasing the particles and exposing them to cavitation [156, 157]. A double wrap in aluminum foils of different thicknesses has been suggested for controlling the release rate [158]. A special feeder device can be used to deliver particles into the cavitation region. Such a system using a worm-type feeder and Ar-atmosphere protection of particles was developed and tried in Mg alloys [159]. The selection of material for the feeding tube is important and maybe cumbersome, especially for aluminum. For Mg alloys, steel can be used.

The delivery of particles in the cavitation region can be also achieved using perforated container (e.g. from Nb) placed underneath the sonotrode [160]. In this case the geometry of the container, the number and size of holes control the release rate.

A next logical step would be to use a kind of master alloy containing a metallic matrix with large concentration of particles, similar to grain refining rods. The particles can be spatially distributed in such a composite master alloy and wetted by the matrix. The master alloy can be produced by a powder metallurgy route, using mechanical alloying for mixing and hot extrusion for consolidation and better particle distribution. Such a scheme was first suggested in the 1960s and implied the direct contact of a sintered aluminum powder (SAP) rod with the sonotrode [47]. Later this approach was used in grain refining practice and tried in MMNC processing [154, 161, 162].

The application of hollow sonotrodes has been also suggested for introduction of the particles into the melt and in the cavitation region [47, 163, 164].

All these techniques are currently tried on the laboratory scale and, obviously, have advantages and disadvantages. The finer the particles, the more complicated their introduction to the melt is. In the case of microscopic (5–100 μm) particles, mechanical or electromagnetic mixing with subsequent or simultaneous ultrasonic processing is sufficient [153, 165].

Most of successful experiments are performed under conditions of developed cavitation with amplitudes 10 to 40 μm at frequencies 17–22 kHz. It seems that there is a consensus that cavitation is the basis of successful ultrasonic processing of composites, especially at the stage of wetting and deagglomeration. Physical modeling using transparent solutions and mixtures and variable ultrasonic parameters (17–20 kHz, 1.4–4 kW) demonstrated that a better distribution of particles in the volume could be achieved at a higher frequency and lower power [166]. In this case the re-agglomeration is prevented and particles are well distributed by acoustic flows in the volume.

Figure 5.23a demonstrates reasonable distribution of alumina nanoparticles in an aluminum alloy, while Fig. 23b shows that USP really result in deaglomeration of nanoparticle agglomerates (evidenced by ultra-small angle X-ray scattering, USAXS).

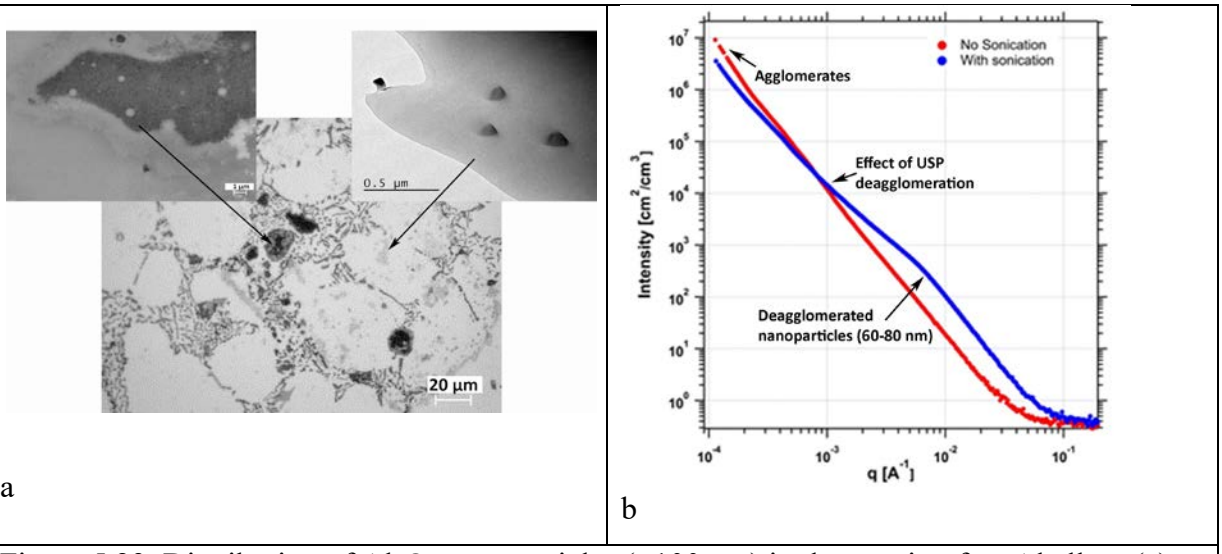

a b

Figure 5.23. Distribution of Al_2O_3 nanoparticles (<100 nm) in the matrix of an Al alloy: (a) metallography with insets showing loose particles in agglomerates (top left) and in the solid solution (top right) (J. Tamayo, W. Lefebvre, D. Eskin, 2015) and (b) USAXS results showing deagglomeration of nanoparticles as a result of USP (courtesy P. Srirangam).

Bearing alloys containing up to 10% Pb (additionally up to 10% Sn, up to 4% Sb) can be produced by the following route [167]. The melt is superheated to 1100–1200 °C that allows for dissolution of 18–30% Pb in liquid aluminum. The melt is then poured through a water-cooled ultrasonic funnel (magnetostrictive transducer arranged around the pouring channel). The ultrasonic processing then occurs simultaneously with melt cooling. This creates conditions for nucleation of Pb droplets under intensive mixing that prevents sedimentation. The process ends with DC casting of billets where high cooling rate helps to preserve the emulsion in the solid state. Lead particles 5–40 µm in size were uniformly distributed in the billet volume.

Another technological approach was suggested by G.I. Eskin [50] and tested under laboratory conditions (casting of a 6XXX-series alloy in a metallic mold 95 mm in diameter, 300 mm in height, processed volume 5 kg). The idea was to avoid addition of the low-melting and immiscible components in the furnace, preventing contamination and necessity for high melt superheat. Relatively small (up to 6%) additions of such elements were done using a master alloy or pure-metal rod with ultrasonic processing in the launder.

The same approach was used in DC casting of a 6XXX-series alloy with addition of Pb in the melt flow with simultaneous ultrasonic processing of the melt [84].

References

[1] Lord Rayleigh, Phil. Mag., 1917, vol. 34, pp. 94–98.

[2] W.J. Altberg, Zh. Rus. Fiz. Khim. Obshch., 1903, vol. 34, pp. 459–460.

[3] Ya.I. Frenkel. Kinetic Theory of Liquids, Moscow, Izd. Akad Nauk SSSR, 1945, 424 p. (Translated in English by New York, Dover Publ., 1955)

[4] E. N. Harvey, D. K. Barnes, W. D. McElroy, A. H. Whiteley, D. C. Pease, K. W. Cooper, J. Cell. Comp. Physiol., 1944, vol. 24, pp. 1–22, 23–34.

[5] B.E. Nolting, E.A. Neppiras. Proc. Royal Soc. London, 1950, vol. 63B, p. 674-685.

[6] Y. Kikuchi, H. Shimizu, J. Acoust. Soc. Am., 1959, vol. 31, pp. 1385–1386.

[7] L.D. Rozenberg, M.G. Sirotyuk, Akust. Zh., 1960, vol. 6, pp. 478–481.

[8] R.W.Wood, A.L. Loomis, Phil. Mag., 1927, vol.4, pp. 417–425.

[9] R.T. Knapp, A. Hollander, Trans. ASME, 1948, vol. 70, pp. 419–435;

[10] A.T. Ellis, Cavitation in Hydrodynamics, Proc. Nat. Phys. Lab. Symp., 1955, London, Her Majesty's Stationery Office, 1956, paper 8.

[11] A.T. Ellis, M.E. Fourney, Proc. IEEE, 1963, vol. 51, pp. 942–943.

[12] R.T. Knapp, Trans. ASME, 1955, vol. 77, pp. 1045–1054.

[13] J. Schmid, Acustica, 1959, vol. 9, pp. 321–326.

[14] M.G. Sirotyuk, Akust. Zh., 1962, vol. 8, p. 216–219.

[15] H. Huang, D. Shu, Y. Fu, J. Wang, B. Sun, Ultrason. Sonochem., 2014 vol. 21, pp. 1275–1278.

[16] W.W. Xu, I. Tzanakis, P. Srirangam, W.U. Mirihanage, D.G. Eskin, A.J. Bodey, P.D. Lee, Ultrason. Sonochem., 2016, vol. 31, pp. 355–361.

[17] D. Tan, T.L. Lee, J.C. Khong, T. Connolley, K. Fezzaa, J. Mi, Metall. Mater. Trans. A, 2015, vol. 46A, pp. 2851–2861.

[18] D.K. Chernov, Zapiski Imperat. Russ. Teckhnich. Obshch., 1879, no. 1, pp. 1–24.

[19] G.F. Balandin, Formation of Crystal Structure in Castings, Moscow, Mashinostroenie, 1973, pp. 192–261.

[20] J. Campbell, Int. Met. Rev., 1981, no. 2, pp. 71–108.

[21] E.A. Hiedemann, J. Acoust. Soc. Am., 1954, vol. 26, pp. 831–842.

[22] G.I. Eskin, Ultrasound in Metallurgy, Moscow, Metallurgizdat, 1961, 47 p.

[23] G.I. Eskin. Ultrasonic Treatment of Molten Aluminum, Moscow, Metallurgiya, 1965, 224 p.
[24] H.G. Flynn, Physics of Acoustic Cavitation in Liquids, in: Physical Acoustics, vol.1, part B, ed. W.P. Mason, New York, Academic Press, 1964, pp. 57–172.
[26] O.V. Abramov, I.I. Teumin, Crystallization of Metals, in: Physical Principles of Ultrasonic Technology, ed. L.D. Rozenberg, Moscow, Nauka, 1970, pp. 427–514 (Translated by New York, Plenum, 1973).
[27] O.A. Kapustina, Degassing of Liquids, in: Physical Principles of Ultrasonic Technology, ed. L.D. Rozenberg, Moscow, Nauka, 1970, pp. 253–336 (Translated by New York, Plenum, 1973).
[28] O.V. Abramov, Crystallization of Metals in an Ultrasonic Field, Moscow, Metallurgiya, 1972, 256 p.
[29] K. Buxmann, Z. Metallkde., 1972, vol. 68, pp. 516–521.
[30] H.J. von Seemann. Metallwirtschaft, 1936, vol. 15, pp. 1067-1069.
[31] H.J. von Seemann, H. Menzel, 1947, Metall, vol. 1, pp. 39–46.
[25] H.J. von Seemann, H. Staats, K.G. Pretor, Arch. Eisenhüttenwesen, 1967, vol. 38, pp. 257–265.
[32] G. Schmid, L. Ehret, Z. Electrochem., 1937, vol. 43, pp. 869–874.
[33] G. Schmid, A. Roll, Z. Electrochem, 1939, vol. 45, pp. 769–775.
[34] R.Ya. Berlaga, Zh. Eksperim. Teor. Fiz., 1939, vol. 9, pp. 1397–1398.
[35] V.I. Danilov, E.E. Pluzhnik, B.M. Teverovsky, Zh. Experim. Teor. Fiz., 1939, vol. 9, pp. 66–71.
[36] V.I. Danilov, B.M. Teverovsky, Zh. Experim. Teor. Fiz. 1940, vol. 10, pp. 1305–1310.
[37] V.J. Altberg, V. Lavrov, Acta Physicochem. USSR, 1939, vol. 11, pp. 287–290.
[38] J.D. Hunt, K.A. Jackson, J. Appl. Phys., 1966, vol. 31, pp. 254–257.
[40] A.E. Ansyutina, I.I. Gur'ev, G.I. Eskin, Izv. Akad. Nauk SSSR, Met., 1970, no. 4, pp. 76–81.
[39] H.J. von Seemann, F. Wehner, Metallwissehschaft und Technik, 1973, vol. 27, pp. 971–977.
[41] D.H. Lane, J.W. Canningham, W.A. Tiller, Trans. Metal. Soc. AIME, 1960, vol. 218, pp. 985–990.
[42] F.F. Benua, I.V. Vologdin, A.I. Katler, Svarochn. Proizvod., 1958, no. 5, pp. 1–5.
[43] V. Boajarevics, G.S. Djambazov, K.A. Pericleous, Metall. Mater. Trans. A, 2015, vol. 46A, pp. 2884–2892.

[44] O. Lindström, J. Acoust. Soc. Am., 1955, vol. 27, pp. 654–671.
[45] V. Becker, Novosti Teckhniki, 1941, vol. 10, no. 4, pp. 25–26.
[46] G.I. Pogodin-Alekseev, V.V. Zaboleev-Zotov, Litein. Proizvod., 1958, no. 7, pp. 35–36.
[47] H.J. von Seemann, H. Staats, Z. Metallde., 1968, vol. 59, pp. 347–356.
[48] E. Herrmann, Handbuch des Stranggiessens, Dusseldorf, Aluminium Verlag, 916 p.
[50] G.I. Eskin, Ultrasonic Treatment of Molten Aluminum, Moscow, Metallurgiya, 1988, 232 p.
[51] S. Komarov, K. Oda, Y. Ishiwata, N. Dezhkunov, Ultrason. Sonochem., 2012, vol. 20, pp. 754–761.
[52] I. Tzanakis, M. Hodnett, G.S.B. Lebon, N. Dezhkunov, D.G. Eskin, Sensors and Actuators A: Physical, 2016, vol. 240, pp. 57–69.
[53] I. Tzanakis, G.S.B. Lebon, D.G. Eskin, K. Pericleous, J. Mater. Process. Technol., 2016, vol. 229, pp. 582–586.
[54] G.S. B. Lebon, I. Tzanakis, G. Djambazov, K. Pericleous, D.G. Eskin, Ultras. Sonochem., 2017, vol. 37, pp. 660–668.
[55] I. Tzanakis, G.S.B. Lebon, D.G. Eskin, K. Pericleous, Materials and Design, 2016, vol. 90, pp. 979–983.
[56] L.D. Rozenberg (ed.). High-Intensity Ultrasonic Fields, Moscow, Nauka, 1968, 267 p. (translated to English by New York, Plenum, 1971)
[57] I. Tzanakis, G.S.B. Lebon, D.G. Eskin, K.A. Pericleous . Ultrason. Sonochem., 2017, vol. 34, pp. 651–662
[58] L. Bergmann, Der Ultraschall und seine Anwendung in Wissenschaft und Technik, 6th Edn., Zürich, S. Hirzel Verlag, 1954, 1114 p.
[59] H. B. Briggs, J. B. Johnson, W. P. Mason, J. Acoust. Soc. Am., 1947, vol. 19, pp. 664–677.
[60] W. Connolly, F.E. Fox, J. Acoust. Soc. Am., 1954, vol. 26, pp. 843–848.
[62] M.S. Plesset, A. Prosperetti, Ann. Rev. Fluid Mech., 1977, vol. 9, pp. 145–185.
[63] D.B. Khismatullin, J. Acoust. Soc. Am., 2004, vol. 116, pp. 1463–1473.
[61] B.E. Noltingk, E.A. Neppiras, Proc. Phys. Soc. London. Sect. B, 1950, vol. 63, pp. 647–685; 1951, vol. 64, pp. 1032–1038.
[64] C.E. Brennen, Cavitation and Bubble Dynamics, Oxford, Oxford University Press, 1995, 304 p.
[65] M. Minnaert, Philos. Mag., 1933, vol. 16, pp. 235–248.

[66] W. Lauterborn, T. Kurz, R. Mettin, C.D. Ohl, Adv. Chem. Phys., 1999, vol. 110, pp. 295–380.

[67] M.M. Fyrillas, A.J. Szeri, J. Fluid. Mech., 1994, vol. 277, pp. 381–407; 1995, vol. 289, pp. 295–314.

[68] L.A. Crum, J. Acoust. Soc. Am., 1980, vol. 68, pp. 203–211.

[69] G.S.B. Lebon, I. Tzanakis, K. Pericleous, D.G. Eskin, Phys. Rev. E, 2015, vol. 92, 043004-1–043004-8.

[70] R. W. Boyle, Trans. Royal Soc. Canada, 3rd Series, 1922, vol. 16, pp. 157–162.

[71] F. Krüger, German Patent no. 604486, 1931; Glastech. Ber., 1938, no.7, pp. 233–236.

[72] H. Eisenreich, Die Technik, 1950, vol. 5, pp. 310–315.

[73] M.B. Altman, D.V. Vinogradova, V.I. Slotin, G.I. Eskin, Izv. Akad. Nauk SSSR, Otd. Tekhn. Nauk, 1958, no. 9, pp. 25–30.

[74] L.A. Arbuzova, K.I. Slovetskaya, A.M. Rubinshtein, L.L. Kunin, V.A. Danilkin, Izv. Akad. Nauk SSSR, Khimiya, 1971, no. 1, pp. 169–170.

[75] P.D. Waite, Light Metals 1998, ed. B. Welch, Warrendale, PA,TMS, 2009, pp. 791–796.

[76] W.R. Opie, N.J. Grant, Trans. AIME, 1950, vol. 188, pp. 1237–1241.

[77] G.S. Makarov, Cleaning of Aluminum Alloys by Gases, Moscow, Metallurgiya, 1983, 119 p.

[78] V.I. Dobatkin, R.M. Gabidullin, B.A. Kolachev, G.S. Makarov, Gases and Oxides in Wrought Aluminum Alloys, Moscow, Metallurgiya, 1976, pp. 65–90.

[79] N. Alba-Baena, D.G. Eskin, Light Metals 2013, ed. B. Sadler, Warrendale, TMS/Wiley, 2013, pp. 958–962.

[80] J. Campbell, Castings, 2nd revised edition, Oxford, UK, Butterworth-Heinemann Ltd, 1993, 352 p.

[81] G.I. Eskin, Ultrasonic Degassing of Molten Metal, Moscow, Mashinostronie, 1968. 39 p.

[82] Y.L. Li and T.G. Zhou, Metall. Mater. Trans. A, 2013, vol. 44A, pp. 3337-3343.

[83] A. Polacovic, P. Sebo, J. Ivan, Z. Augustinicova, Ultrasonics, 1978, vol. 16, pp. 210–212.

[84] G.I. Eskin, D.G. Eskin. Ultrasonic Treatment of Light Alloy Melts. The 2nd Edn., Boca Raton, CRC Press, 2015.

[85] O.V. Abramov, High-Intensity Ultrasonics. Theory and Industrial Applications, Amsterdam, OPA Gordon and Breach, 1998, pp. 291–313.

[86] P.P. Prokhorenko, N.V. Dezhkunov, G.E. Konovalov, Ultrasonic Capillary Effect, Minsk, Nauka i Tekhnika, 1981, 140 p.

[87] Yu.I. Kitaigorodsky, V.I. Drozhalova, In Application of Ultrasound in Metallurgy, Trans. Moscow Inst. Steel and Alloys, 1977, no. 90, pp. 12–16.

[88] N.V. Malykh, V.M. Petrov, In Proc. XIII Session Rus. Acoust. Soc., Moscow, Russian Acoustical Society, 2003, pp. 41–44.

[89] I. Tzanakis, W.W. Xu, D.G. Eskin, P.D. Lee, N. Kotsovinos, Ultrason. Sonochem., 2015, vol. 27, pp. 72–80.

[90] V.I. Danilov, Constitution and Crystallization of Liquids, Kiev, Izd. Akad. Nauk SSSR, 1956, 424 p.

[91] V.I. Danilov, V.E. Neimark, Zh. Eksper. Teor. Fiz., 1949, vol. 19, pp. 235–241.

[92] O.D. Kazachkovsky, in: Collective Papers of the Laboratory of Metals Physics, ed. V.I. Danilov, Kiev, Izd. Akad. Nauk UkrSSR, 1948, pp. 103–112.

[93] G. M. Swallowe, J. E. Field, C. S. Rees, A. Duckworth, Acta Mater., 1989, vol. 37, pp. 961–967.

[94] R. Chow, R. Blindt, R. Chivers, M. Povey, Ultrasonics, 2005, vol. 43, pp. 227–230.

[95] F. Wang, D. Eskin, J. Mi, T. Connolley, M. Mounib, J. Lindsay, Acta Materialia, 2016, vol. 116, pp. 354–363.

[96] F. Wang, D. Eskin, T. Connolley, C. Wang, B. Koe, A. King, C. Reinhard, J. Mi, Scr. Mater., 2018 (submitted).

[97] N.I. Chvorinov, Crystallization and Non-Homogeneity of Steel, Prague, Publishing House of Czechoslovak Academy of Sciences (NČSAV), 1954, 384 p.

[98] A. Vogel, R.D. Doherty, B. Cantor, in: Solidification and Casting of Metals, London, TMS, 1979, pp. 518–25.

[99] K.A. Jackson, J.D. Hunt, D.R Uhlmann, T.P. Seward, Trans. Metall. Soc. AIME, 1966, vol. 236, pp. 149–160.

[100] A.A. Chernov, Kristallografiya, 1956, vol. 1, pp. 589–593.

[101] T. Z. Kattamis, J. C. Coughlin, M. C. Flemings, Trans. Metall. Soc. AIME., 1967, vol. 239, pp. 1504–1511.

[102] D. Ruvalcaba, R.H. Mathiesen, D.G. Eskin, L. Arnberg, L. Katgerman, Acta Mater., 2007, vol. 55, pp. 4287–4292.

[103] F. Wang, D. Eskin, T. Connolley, J. Mi, C. Wang, B. Koe, A. King, C. Reinhard. Acta Mater., 2017 (submitted).

[104] D. Shu, B. Sun, J. Mi, P.S. Grant, Metall. Mater. Trans. A, 2012, vol. 43A, pp. 3755–3766.

[105]. F. Wang, I. Tzanakis, D. Eskin, J. Mi, T. Connolley, Ultrason. Sonochem., 2017, vol. 39, pp. 66-76.

[106] T.V. Atamanenko, D.G. Eskin, L. Zhang, L. Katgerman. Metall. Mater. Trans. A, 2010, vol. 41A, pp. 2056–2066.

[107] P.P. Bhingole, G.P. Chaudhari, Mater. Sci. Eng. A, 2012, vol. 556, pp. 954–961.

[108] V.M. Sreekumar, N.H. Babu, D.G. Eskin, Metall. Mater. Trans. B, 2017, vol. 48B, pp. 208–219.

[109] J.A. Dantzig, M. Rappaz, Solidification, Lausanne, Boca Raton, EPFL, CRC Press, 2009, pp.51–56; 268–275.

[110] H. Rumpf, Agglomeration, ed. W.A. Knepper, New York, NY, John Wiley, 1962, pp. 382–403.

[111] S.G. Bochvar, G.I. Eskin, Tekhnol. Legk. Spl., 2012, no. 1, pp. 9–17.

[112] O.B. Kudryashova, D.G. Eskin, A.P. Khrustalev, S.A. Vorozhtsov, Izv. Vyssh. Uchebn. Zaved., Poroshkov. Metall. Funkts. Pokryt., 2016, no. 3, pp. 43–50.

[113] T.V. Atamanenko, D.G. Eskin, L. Zhang, L. Katgerman, Metall. Mater. Trans. A, 2010, vol. 41A, pp. 2056–2066.

[114] T.V. Atamanenko, D.G. Eskin, M. Sluiter, L. Katgerman, J. Alloys and Compounds, 2011, vol. 509, no. 1, pp. 57–60.

[115] F. Wang, D. Eskin, T. Connolley, J. Mi J. J. Cryst. Growth, 2016, vol. 435, pp. 24–30.

[116] F. Wang, D. Eskin, T. Connolley, J. Mi, Trans. Nonferr. Met. Soc. China, 2017, vol. 27, pp. 977−985.

[117] G. Wang, M.S. Dargusch, M. Qian, D.G..Eskin, D.H..StJohn, J. Cryst. Growth, 2014, vol. 408, pp. 119–124.

[118] R.W.Wood, A.L. Loomis, Phil. Mag., 1927, vol.4, pp. 417–425.

[119] W.T Richards, J. Am. Chem. Soc., 1929, vol. 51, pp. 1724–1729.

[120] C. Bondy, K Söllner, Trans. Faraday Soc., 1935, vol. 31, pp. 835–842.

[121] S.A. Neduzhy, Akust. Zh., 1961, vol. 7, pp. 275–294.

[122] S.A. Neduzhy, Aksut. Zh., 1964, vol. 10, pp. 456–464.

[123] B. Abismaïl, J.P. Canselier, A.M. Wilhelm, H. Delmas, C. Gourdon, Ultrason. Sonochem., 1999, vol. 6, pp. 75–83.

[124] O. Behrend, K. Ax, H. Schubert, Ultrason. Sonochem., 2000, vol. 7, pp. 77–85.

[125] O. Behrend, H. Schubert, Ultrason. Sonochem., 2001, vol. 8, pp. 271–276.

[126] W. Zhai, H.M. Liu, B. Wei, Mater. Lett., 2015, vol. 141, pp. 221–224.

[127] W. Zhai, B.J. Wang, H.M. Liu, L. Hu, B. Wei, Sci. Rep., 2016, vol 6, Paper 36718.
[128] M. da Silva, L. Rebolledo, T. Pabel, T. Petkov, X. Planta, J. Tort, D. Eskin, Int. J. Cast Metals Res., 2015, vol. 28, no. 4, pp.193–200.
[129] V.A. Livanov, G.I. Eskin, N.A. Genisaretsky et al., Tsvetn. Met., 1968, nol. 6, pp. 82–84.
[130] G.I. Eskin, P.N. Shvetsov, in Metals Science and Casting of Light Alloys, Moscow, Metallurgiya, 1977, pp. 8–17.
[131] D.G. Eskin, K. Al-Helal, I. Tzanakis, J. Mater. Proc. Technol., 2015, vol. 222, pp. 148–154.
[132] Q. Han, H. Xu, T.T. Meek, Degassing of molten alloys with the assistance of ultrasonic vibration, US Patent 7682556 B2, 23.03.2010.
[133] V.Rundquist, K.Manchiraju,Q.Han, in Light Metals 2015, ed. M. Hyland, Warrendal: TMS/Wiley, pp. 943–948.
[134] J.H. Grandfield, D.G. Eskin, I.F. Bainbridge, Direct-Chill Casting of Light Alloys. Science and Technology, Hoboken, John Wiley and Sons, 2013, p. 412.
[135] I.I. Novikov, Hot Shortness of Non-Ferrous Metals and Alloys, Moscow, Nauka, 1966, 299 p.
[136] D.G. Eskin, Suyitno, L. Katgerman. Progr. Mater. Sci., 2004, vol. 49, no. 5, pp. 629–711.
[137] V.A. Livanov, R.M. Gabidullin, V.S. Shepilov. Continuous Casting of Aluminum Alloys, Metallurgiya, Moscow, 1977, 168 p.
[138] I.L. Teitel. In Wrought Aluminum Alloys, ed. I.N. Fridlyander, V.I. Dobatkin, E.D. Zakharov, Oborongiz, Moscow, 1961, pp. 200–209.
[139] V.I. Dobatkin, G.I. Eskin, S.I. Borovikova, Fiz. Khim. Obrab. Mater., 1973, no. 6, pp. 37–41.
[140] V.I. Dobatkin, G.I. Eskin, Tsvetn. Met., 1991, no. 12, pp. 64–67.
[141] G.I. Eskin, Z. Metallkde., 2002, vol. 93, pp. 503–507.
[142] G.I. Eskin, D. G Eskin, Mater. Sci. Forum, 2002, vols. 396–402, pp. 77–82.
[143] G.I. Eskin, P.R. Silayev, In Processes of Treatment of Light and High-Temperature Alloys, Moscow, Nauka, 1981, pp. 118–122.
[144] V.K. Yunyshev, G.I. Eskin, P.R. Silayev, Tekhnol. Legk. Spl., 1981, no. 2, pp. 26–30.
[145] G. Salloum-Abou-Jaoude, D.G. Eskin, C. Barbatti, P. Jarry, M. Jarrett, Z. Fan, Light Metals 2017, Ed. Arne P. Ratvik, TMS/Springer, pp. 997-1003.

[146] V.M. Sreekumar, D.G. Eskin, JOM, 2016, vol. 68, pp. 3088–3093.
[147] J.C. Hoff, US Patent 3,634,075; 1970.
[148] D.A. Granger, In Light Metals 1998, ed. B. Welch, Warrendale, TMS, 1998, pp. 941–952.
[149] A.L Greer, A.M Bunn, A Tronche, P.V Evans, D.J Bristow, Acta Mater., 2000, vol. 48, pp. 2823–2835.
[150] G.I. Eskin, A.A. Rukhman, S.G. Bochvar, V.I. Yalfimov, D.V. Konovalov, Tsvetn. Met., 2008, nol. 3, pp. 105–110.
[151] G.I. Eskin, S.G. Bochvar, V.I. Yalfimov, Tekhnol. Legk. Spl., 2010, no. 1, pp. 38–43.
[152] A.I. Kolmakov, V.I. Silaeva, T.V. Solov'eva, G.I. Eskin, In Application of Ultrasound in Industry, Alma-Ata, NTO Mashprom, 1972, pp. 21–24.
[153] G.I. Eskin, D.G. Eskin, Ultrason. Sonochem., 2003, vol. 10, pp. 297–301.
[154] Y.Yang, X. Li, J. Manuf. Sci. Eng., 2007, vol. 129, pp. 497–501.
[155] G. Cao, H. Konishi, X. Li, Mater. Sci. Eng. A, 2008, vol. 486, pp. 357–362.
[156] I.I. Sidorin, V.I. Silaeva, T.V. Solov'eva, V.I. Slotin, G.I. Eskin, Metalloved. Termich. Obrab. Met., 1971, no. 8, pp. 23–26.
[157] G.I. Eskin, Tekhnol. Legk. Spl., 1974, no. 11, pp. 21–25.
[158] H. Choi, M. Jones, H. Konishi, X. Li, Metall. Mater. Trans. A, 2012, vol. 43A, pp. 738–746.
[159] H. Choi, Y. Sun, B.P. Slater, H. Konishi, X. Li, Adv. Eng. Mater., 2012, vol. 14, pp. 291–295.
[160] S. Nimityuongskul, M. Jones, H. Choi, R. Lakes, S. Kou, X. Li, Mater. Sci. Eng. A, 2010, vol. 527, pp. 2104–2111.
[161] D. Wang, M.P. De Cicco, X. Li, Mater. Sci. Eng. A, 2012, vol. 532, pp. 396– 400.
[162] S.A. Vorozhtsov, D.G. Eskin, J. Tamayo, A.B. Vorozhtsov, V.V. Promakhov, A.A. Averin, A.P. Khrustalyov, Metall. Mater. Trans. A, 2015, vol. 46A, July, pp. 2870–2875.
[163] H.J. von Seemann, H. Staats, German Patent DE1126074(B), publ. 22.03.1962.
[164] G.I. Eskin, P.N. Shvetsov, USSR Invention Certificate 246060, publ. 01.01.1969.
[165] Y. Tsunekawa, H. Sizuki, Y. Genma, Mater. Design, 2001, vol. 22, pp. 467–472.
[166] L. Shiying, G. Feipeng, Z. Qiongyuan, L. Wenzhen, Mater. Sci. Forum, 2009, vols. 618–619, pp. 433–436.
[167] O.V. Abramov, Influence of Powerful Ultrasound on Liquid and Solid Metals, Moscow, Nauka, 2000, pp. 142–163.